University of Calgary

PRISM Repository **https://prism.ucalgary.ca**

The Vault Open Theses and Dissertations

2017-12

Flowback Study of Hydraulic Fracturing in Shale Gas Reservoirs

Jing, Gui Cheng

Jing, G. (2017) Flowback Study of Hydraulic Fracturing in Shale Gas Reservoirs (Master's thesis, University of Calgary, Calgary, Canada). Retrieved from https://prism.ucalgary.ca. http://hdl.handle.net/1880/106255

Downloaded from PRISM Repository, University of Calgary

UNIVERSITY OF CALGARY

FLOWBACK STUDY OF HYDRAULIC FRACTURING IN SHALE GAS RESERVOIRS

by

GUICHENG JING

A THESIS

SUBMITTED TO THE FACULTY OF GRADUATE STUDIES

IN PARTIAL FULFILMENT OF THE REQUIREMENTS FOR THE

DEGREE OF MASTER OF SCIENCE

GRADUATE PROGRAM IN CHEMICAL AND PETROLEUM ENGINEERING

CALGARY, ALBERTA

DECEMBER, 2017

© GUICHENG JING 2017

Abstract

Shale gas production has achieved great success in the U.S.A and Canada. It is increasingly critical in reshaping the global energy landscape. Multi-stage hydraulic fracturing in horizontal wells is widely accepted as the most economic and effective technique to unlock shale gas reservoirs. As shale gas production continues, higher requirements are proposed to improve the long-term productivity after hydraulic fracturing. Fracture cleanup after hydraulic fracturing is an important factor to impacting long-term production forecasting. It plays a significant role in optimizing flowback of a fracturing fluid to maintain the optimal conductivity in hydraulic fractures.

This research is focused on the development of a novel simulator using a mathematical model to optimize a choke size as wellhead pressure changes over time. This new optimization model is capable of performing dynamic adjustment of a choke size while wellhead pressure changes over time. It has a two-phase (gas and liquid) flow model along the horizontal, slanted and vertical sections as fractures close. The model simultaneously considers forces acting on proppant particles, filtration loss of water, compressibility of the fracturing fluid, wellbore friction, a gas slippage effect, water absorption and adsorption. The theoretical feasibility of gas releasing from shale faces when the pressure in fractures is greater than the formation pressure is identified due to the capillary pressure and substitution. Using an idealized straight smooth capillary model, the join forces of capillary pressure and formation pressure are greater than the pressure in fractures in the non-water-wetting section allowing the gas to move and be produced. In order to maximize flowback of the fracturing fluid to the surface and the volume of proppants remaining in the fractures, this research determines the

maximum flow velocity of the liquid based on the forces acting on proppant particles. To build the optimization model, the equations of a pressure drop in the two-phase (gas and liquid) flow were derived considering a slippage effect and friction loss while temperature and/or pressure alter along the horizontal, slanted and vertical wellbores. After investigating the workflow of hydraulic fracturing and fracture cleanup, the interface and functions of the novel simulator were designed. The interface is realized with QT and operated by coding with C++ language. The flowback section is complete and a novel simulator testing procedure has been applied to a shale gas well from the Shuangyang Formation in China. Comparison curves with both real and simulation data are demonstrated respectively. Both real and simulation data have the identical changing tendencies and match each other very well.

Keywords: flowback, shale gas reservoir, multi-stage hydraulic fracturing, choke size optimization, two-phase flow, wellbore friction, gas slippage effect, simulator development

Acknowledgements

I want to express my gratitude to my supervisor Dr. Zhangxing (John) Chen, who has provided valuable instructions, support and suggestions to guide my research and study.

I would like to thank Ms. Jenny Zhang, Mr. Fei Li and Dr. Yongli Wang, who gave me valuable suggestions on my theoretical research and simulator development.

I would like to thank Mr. Lu at Jilin Oilfield Corporation, who provided me with reference data and advised me on my thesis.

Thanks also go to my friends and colleagues and the department faculty and staff in the Department of Chemical and Petroleum Engineering , Schulich School of Engineering for making my time at the University of Calgary a great experience.

Finally, thank you, my family, for your encouragement, support, patience and love!

Dedication

With sincerity, love and affection, my work is dedicated to my supervisor, committee members and my family!

Table of Contents

List of Tables

List of Figures and Illustrations

List of Symbols, Abbreviations and Nomenclature

Symbol	Definition
a	Length, width and height of a small shale cube, m
A_H	Hamaker constant for solid--liquid interactions, J
A_{H^*}	Hamaker constant for liquid-liquid interactions, J
C_f	compressibility coefficient of fluid, including gas and liquid, MPa^{-1}
C_l	lifting force coefficient, dimensionless
d	diameter of wellbore, m
d_s	proppant particle diameter, m
e	number of ions in one mole of solvend
E	Young's Modulus, MPa.
Erfc()	Gauss Error Function
Fc	cohesion force acting on the particle, N;
F_l	lifting force acting on the particle, N
g	gravitational acceleration, 9.80665 m/s^2
H_{fi}	height of No. I fracture, m
K	formation permeability μm^2
L_{fi}	half-length of No. i fracture, m
L_i	distance from the point of No. i fracture to the wellbore bottom (Point II in Figure 3-13), m
L_{i+1}	distance from the point of No. i+1 fracture to the wellbore bottom (Point II in Figure 3-13), m
LS	length of the slanted path, m
m	salinity of solution
n and b	multi-variation constants when the mixture of gas and liquid is flowing through the choke, dimensionless
P_0	setup pressure at the outlet of choke, MPa
P1	pressure at the point of first stage of hydraulic facture, MPa
P2	pressure at the end point of horizontal section, MPa
P_{cap}	capillary pressure, MPa

$P_{fi}(t)$	pressure at the point of No. i fracture in the wellbore at time t, MPa
$P_{fi+1}(t)$	pressure at the point of No. i+1 fracture in the wellbore at time t, MPa
Ps	pressure under standard conditions, 0.10 MPa
$P_{wf(t)}$	pressure at the end point of the horizontal section at any time t, MPa
$P_{wh(t)}$	wellhead pressure at any time t, MPa
P(x,t)	pressure at any time t and at any place x in the formation, MPa; P_R is the formation pressure, MPa
$P_{III(t)}$	pressure at the end point of the slanted section at any time t, MPa
Qgi	gas volume at the point of No. i fracture at time t, m^3/sec
Q_l	liquid volume at time t, m^3/sec
Q_L	volume flow of pure liquid flow, m3/sec
$Q_{ri}(t)$	gas flow rate at time t at the point of No. i fracture in the wellbore, m^3/sec
r	radius of the picked section of capillary throat, m
r_{wa}	water absorption ratio, dimensionless
R	gas constant, J/mol·K
Re	Reynolds number, dimensionless
RH	water saturation in hydraulic fractures, dimensionless
tg	specific time when the gas starts releasing from shale face, sec
T	temperature, K
Ts	standard temperature, 15°C
u_B	threshold velocity of proppant particle's start-up, m/sec
u_{gi}	average flow rate of gas + liquid mixture between the points of No. i and No. i+1 fractures, m/sec
$u_m(t)$	average flow rate of mixture of gas + liquid at time t, m/sec
v_c	flow velocity at the outlet of choke, m/sec
v_{fl1}	filtration loss velocity controlled by the viscosity of the fracturing fluid, m/min
v_{fl2}	filtration loss velocity controlled by total compressibility of the formation fluid
v_{mc}	flow velocity of the mixture of gas and liquid at the outlet of choke at time t, m/sec
$v_r(t)$	velocity of the gas releasing from shale face at time t, $m^3/(m^2.sec)$

Vg	gas volume in a unit mass of gas, m3
V_l	liquid volume in a unit mass of liquid, m^3
V_m	maximum water absorption volume per unit area
V_{mv}	molar volume of water, cm^3/mol
Wo	submerged weight of particle, N
x_L	filtration distance from the fracture face, m
Z	gas compressibility coefficient under standard conditions of P and T, dimensionless
Zs	gas compressibility coefficient under standard conditions, dimensionless
γ	shale's Possion's ratio,dimensionless
Δh	height of vertical path of the wellbore, m
ΔL	length of horizontal section of wellbore, m
ΔP1	pressure difference that causes the filtration loss controlled by the viscosity of fracturing fluid, MPa
ΔP_2	pressure difference which causes the filtration loss controlled by the total compressibility of formation fluid, MPa
$\triangle\zeta$	adopted to depict clay/water film/movable liquid phase interactions when the condition of contact angle is less than 60°, mV
ε_c	cohesion force coefficient among particles, 0.00256 N/m
ε	relative dielectric permittivity of liquid, dimensionless
ε_0	electric constant in a vacuum
ζ_1 and ζ_2	electric potentials of the solid–water film and water film-movable fracture fluid interfaces, respectively, mV
θ	angle between horizontal and slanted sections, dimensionless
θ_{cap}	contact angle among water, gas and rock, dimensionless
θ_o	osmotic coefficient of saline solution
κ	coefficient for the strength of structural force, N/m^2
λ	characteristic length of water molecules, nm
$\lambda(t)$	friction resistance coefficient along the wellbore at time t
μ	apparent viscosity of the fracturing fluid in the fractures under the condition of flowing, mPa.s

μ_l	viscosity of fracturing fluid, mPa.s
ξ	local resistance coefficient when the fluid is flowing through the choke, dimensionless
$\Pi(h)$	disjoining pressure between a solid surface and liquid film, MPa
$\Pi_1(h)$	disjoining pressure between water film and surface on the same side considering both of the short-range (structural force Π_s) and long-range interactions (molecular force Π_m and electrical force Π_e), MPa
$\Pi_2(h)$	disjoining pressure between the water film and the surface on the opposite side. By neglecting short-range interactions (structural force Π_s) due to the relative long range between film and opposite fracture surface, MPa
$\Pi_3(h)$	disjoining pressure between two water films and only considers molecular force Π_m because the potentials difference between the two similar films is zero, MPa
Π_e	electrical force, MPa
Π_m	London–Van der Waals force, MPa
Π_s	structural force, MPa
ρ_{gs}	gas density under standard conditions, 0.717 kg/m^3
ρ_f	density of fracturing fluid, g/cm^3
ρ_m , ρ_g , ρ_l	density of mixture of gas + liquid, the density of gas and the density of liquid at P and T, respectively, kg/m^3
ρ_s	proppant particle density, kg/m^3
σ	surface tension of water and gas, N/m
Ø	formation porosity, fraction
CAPEX	Capital expenditure
DFM	Discrete fracture method
DFN	Discrete fracture network
DPM	Dual porosity flow model
DRP	Dynamic relative permeability

EDFM	Embedded discrete fracture method
FAM	Flow back analytical model
FMB	Flowing material balance
MBE	Material balance equation
nm	nanometer
NMRD	Nuclear magnetic resonance
OPEX	Operational expenditure
RTA	Rate transient analysis
SRV	Stimulated reservoir volume
TRA	Tight rock analysis
TOC	Total organic content
TPR	Time-pressure-rate
U.S.A	United States of America

Chapter 1 INTRODUCTION

1.1 Background

What is multi-stage hydraulic fracturing in horizontal wells? As shown in Figure1-1, a horizontal well with hundreds of meters of a horizontal section is drilled and cemented in the formation underground. A fracturing fluid is a mixture of proppants, water and chemical agents. It is injected into the well under high pressure with a pumper truck. Along with the horizontal section, many packers are pinpointed at diverse locations of perforation to isolate the different stages occurring during fracking. Hydraulic fracturing, or ‘fracking’, involves the injection of thousands of cubic meters of water, proppants and chemical agents at high pressure down and into horizontally drilled wells. After one stage of rock is cracked, it is packed and the next stage is fracked. When rock is fractured, the fracturing fluid enters into fractures. The pressurized fracturing fluid causes the rock layers to crack. The fractures are held open by the proppant particles so that natural gas from the shale can flow up the well. When all the stages of the fracking process are completed, the fracture cleanup is conducted. The fracturing fluid flows back to the surface in a controlled velocity to maximize flowback of the fracturing fluid to the surface and the proppants remaining in the fractures.

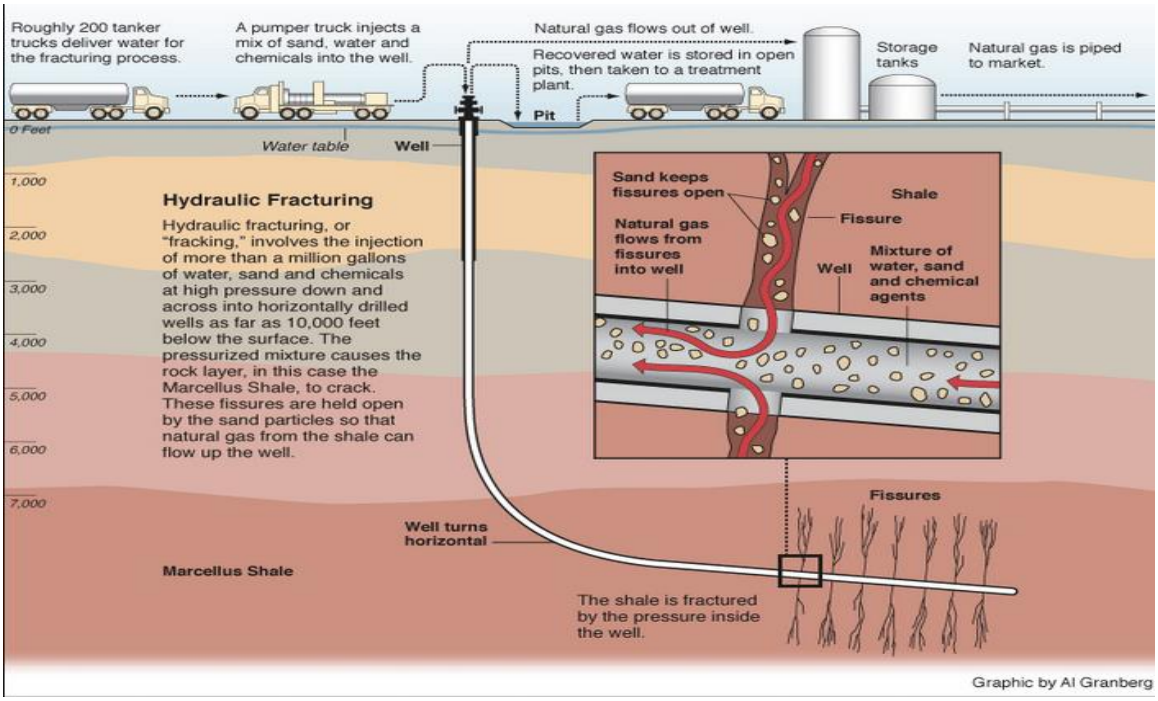

Figure 1-1 Hydraulic fracturing process (Courtesy of Google Picture)

Shale gas is categorized as an unconventional asset, generated from deposited organic matters in mudstone and interlayers. It is mostly stored as adsorption gas and some of the gas is free gas existing in natural fractures and micropores where it accumulates in source rocks after gas generation. It is referred to as the typical "in-situ" reservoir pattern (Zhang J. et al. 2004).

Shale gas has drawn increasing global attention as a reliable energy source with successful recovery in the United States of America (U.S.A) (Exxon Annual Report 2006, Mobil Annual Report 2007). It is believed that multi-stage hydraulic fracturing with slick water in horizontal wells is the most effective and profitable implementation in ultra-low permeable shale gas formations. However, the knowledge of shale gas development is still insufficient; features and behaviors of fracture cleanup need further in-depth research.

Figure1-2 provides a general overview from drilling to production for a shale gas well. Most shale wells are hydraulically fractured in multiple stages, followed by a fracture cleanup and then a shut-in period because there is a delay taking the wells to production. After the fracture cleanup period, the wells continuously produce gas that is available for sale. This is called the production period. A fracturing job begins the flow sequence of a normal shale gas well lifecycle. This is followed by the flowback period with high water and gas rates. The wells start to produce after two to five days. Some wells are shut-in due to a connection delay. Then formal gas production starts.

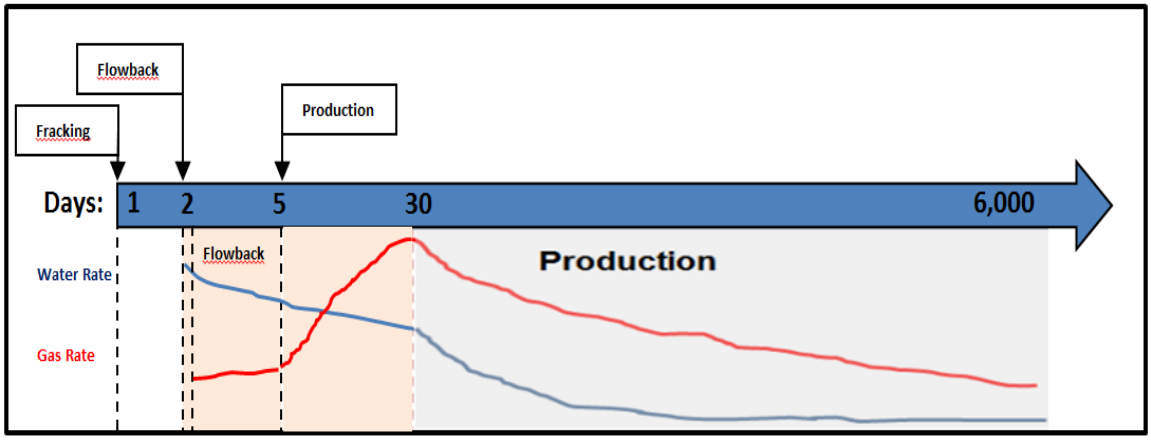

Figure 1-2 Sketch graph of workflow for a usual shale gas well

1.2 Problem Description

Hydraulic fracturing is a well stimulation treatment that involves pumping thousands of barrels of water with proppants and additives into a rock at a pressure greater than the breakdown pressure. A large portion of this fracturing fluid leaks into the formation or is trapped in natural fractures due to the high capillary pressure. Some

of the trapped fluid permeates into the matrix and natural fractures and creates an invasion zone. Some fluid tends to adsorb on fracture surfaces and forms an immovable water film. Chekani et al. (2010) illustrated that only 10-40% of a pumped fracturing fluid flows back (load recovery) to the surface in shale gas wells. 60-90% of the injected fracturing fluid remains in the reservoir. Crafton and Guderson (2007) stated that flowback of fracturing fluids after hydraulic fracturing of multi-stage horizontal shale gas wells impacts long-term production. During hydraulic fracturing flowback operations, only a small portion of the fracturing fluids flow back to the surface. This causes an unconformity between the expected fracture length and the real production fracture length. Determining the optimal choke size during fracture clean-up helps to maximize the conductivity in hydraulic fractures. The choke size is modified by gradually increasing the diameter as the fractures close.

This research is focused on solving the following three questions: (1) What is the optimization model for the dynamic adjustment of a choke size as wellhead pressure changes over time? (2) How can the related simulator be developed with C++ language? (3) What can we do to test the developed simulator with real data from field operations?

1.3 Motivation

Multi-stage hydraulic fracturing in horizontal wells is the most economic and effective technique to unlock shale gas reservoirs because extremely low permeability impedes production. The productivity of a multi-fracked well is correlated with fracture cleanup efficiency. A fracturing fluid may turn into an immovable fluid at high volumes,

causing a slow or incomplete cleanup. To maximize flow-back of the fracturing fluid to the surface and the volume of proppants remaining in the fractures, the optimization of a choke size during the fracture cleanup process is investigated.

There are many commercial software products that model hydraulic fracturing: GOHFER by Barree & Associates LLC, FracproPt by CARBO Ceramics Inc, Mangrove by Schlumberger Ltd, E-StimPlan by NSI Technologies LLC, MFrac by Baker Hughes Inc and FracMan by FracMan Technology Group. In each of these, the optimization of a choke size versus wellhead pressure is oversimplified. The current products take weeks to generate results. A fracturing scheme and a choke size should be adjusted dynamically to new parameters and pressure fluctuations, requiring wellsite engineers to make costly decisions within hours. The tools are insufficient and the impact is that engineers risk millions of dollars relying on guesswork and empirical values. The simulator developed in this research is based on a streamlined mathematical model and the user can obtain an optimized scheme within hours without sacrificing accuracy. By utilizing results from the mathematical modeling of the fracture cleanup rates, this novel simulator can optimize a choke size at varying times and pressures, accounting for critical fracturing including fracture cleanup.

1.4 Research Objectives

The objectives of this work are:

- Build an optimization model for the dynamic adjustment of choke size as wellhead pressure changes over time with a two-phase (gas and liquid) flow model as fractures close along the horizontal, slanted and vertical

sections. The model simultaneously considers the forces acting on proppant particles, filtration loss of water, compressibility of the fracturing fluid, wellbore friction, a gas slippage effect, water absorption and adsorption.

- Investigate the workflow of hydraulic fracturing and fracture cleanup and advance the interface and functions.
- Write the code with C++ language and realize the interface with QT.
- Debug and test developed simulator with real data from field operations.

1.5 Organization of this Thesis

This work is divided into six chapters. The outline and the organization of the thesis are as follows:

Chapter 1 is a brief introduction of this thesis comprised of research background, problem description, motivation and research objectives.

Chapter 2 has a literature review that provides a roadmap for the development of the hydraulic fracturing technology, summarizes current research and application situations of fracture cleanup and choke size optimization and field operations, and finally looks at the current commercial fracturing software.

Chapter 3 focuses on building the optimization model for the dynamic adjustment of a choke size as wellhead pressure changes over time with two-phase (gas and liquid) flow model along the horizontal, slanted and vertical sections. It simultaneously considers forces acting on proppant particles, filtration loss of water, compressibility of

the fracturing fluid, wellbore friction, a gas slippage effect, water absorption and adsorption.

Chapter 4 presents the simulator development with C++ code and interface realization with QT using the proposed methodology.

Chapter 5 validates the developed simulator with real shale gas reservoir data from field operations in China.

Chapter 6 contains the conclusions and recommendations for future work.

Chapter 2 REVIEW OF LITERATURE

2.1 Introduction

This chapter presents a comprehensive roadmap of hydraulic fracturing technology development. The Barnett shale gas fracturing technology provides an example of the growing tendency to use fracking globally. A review of principal current papers and the state of fracture cleanup and choke size optimization and field operation are depicted. A review of papers that consider the current commercial fracturing software briefly explores their advantages and disadvantages. A subtotal for the literature review is stated at the close of this chapter.

2.2 Hydraulic fracturing technology progress

Over the last three decades, there has been a technical renovation facilitating the development of a viable commercial process for shale gas production. National policies in U.S.A support the technical advances and have provided an environment to develop the rapid recovery of shale gas (Li, X., et al. 2007). The technical innovations have arisen in an environment of rapid development of new drilling and completion technique, and the evolution of the hydraulic fracturing technology. From the pioneering nitroglycerin explosion method to the newest synchrotron fracturing technique, the development of well stimulation technologies have significantly improved the recovery effectiveness of shale gas (Ma, C. et al. 2011).

Gandossi, L. et al. (2015) provided an overview of the historical progression of the fracturing technology. The first attempt at fracking used a nitroglycerin blast in a vertical open hole in the 1970s. The result was major damage to the wellbore and the

scope of formation cracks was extremely limited. In 1981, the fracturing techniques of nitrogen or CO_2 foam was put into use in several vertical wells in shale gas formations. The outcome was that formation damage was reduced and shale gas production was increased by three to four times. A cross-linked gel (a thickening or crosslinking agent) was used in the fracturing fluid system during the 1980s and most of the 1990s. This was followed in 1992 with the first horizontal well of shale gas in the HAMETT basin in the U.S.A. Since that time, little by little, horizontal wells have replaced the usage of vertical wells in shale gas development. The hydraulic fracturing technology in horizontal wells was determined to be effective in creating fracture networks and enlarging a natural gas drainage area. This resulted in increased oil and gas recovery and reduced costs. The advance of large-scale multi-fracked horizontal wells has made a great contribution to the economic production of shale gas assets.

Jaripatke et al. (2010) summarized the historical process and roadmap of shale gas production and the advance of drilling and completion technologies in the Barnett Basin in the U.S.A, as shown in Table 2-1. In their paper, they described, in 1998, how the hydraulic fracturing technique for shale gas recovery made a breakthrough; a fracturing fluid can be a water-based liquid (slick water), not only a gel. The new fracturing fluid was primarily water with a lower sand ratio. The proppants usage was about 90% less than the previous gel fracturing fluid. The expenditure of this fracturing fluid decreased by more than 50% and generated better fracturing behavior improving the recovery efficiency by more than 30%.

The multi-stage hydraulic fracturing technique for horizontal wells was developed quickly after 2000 and the mercantile prospect of shale gas exploitation continues to be

promising. Multi-stage hydraulic fracturing has been continuously improved. It has gone from two stages to 20+ stages. The discharge area and recovery efficiency have increased significantly. The application of the multi-stage hydraulic fracturing technology in horizontal wells for the development of shale gas in the U.S.A has increasingly become the standard methodology. It is utilized in over 85% of new drilled horizontal wells (Xu, et al. 2015).

The incorporation of the microseismic fracture monitoring technology and multi-stage hydraulic fracturing in horizontal wells became the principal technique in 2005. It is applied in the recovery of shale gas assets. This was quickly integrated into a novel hydraulic fracturing technology: Synchronous Fracturing Technology in 2006. It is being utilized in the Barnett shale gas basin to this day (Jaripatke et al. 2010).

Table 2 - 1 The advances of Barnett shale gas stimulation. (Jaripatke et al. 2010)

Phase	**Period**	**Accumulated Well Number**	**Fracturing Technology**
Initial	1979	5	High energy gas fracturing
	1981	6	N_2，CO_2 foam fracturing
	1984	17	Cross linked gel fracturing,liquid quantity 100000gal（378m^3）
	1985	49	Cross linked gel fracturing,liquid quantity 500000gal（1892m^3）
	1988	62	Cross linked gel fracturing
	1991	96	Horizontal well and cross linked gel fracturing
	1995	200	Horizontal well fracturing and Cross linked gel fracturing
	1997	300	Riverfracing treatment, liquid quantity 500000gal(1892m^3）
	1999	450	Riverfracing treatment, inclinometer fracture monitor
	2001	750	Riverfracing treatment, micro seismic fracture monitor
	2002	1700	Horizontal well fracturing, Riverfracing treatment
Development	2003	2600	New well with 85 horizontal wells，117 directional wells，719 vertical wells
	2004	3500	150 wells with horizontal well stage fracturing， 2-4 stages
	2005	4500	600 new horizontal wells drilling time is greatly reduced
	2006	5500	Synchronous fracturing,lower development costs
	2007	7000	Horizontal well fracturing, synchronous fracturing
	2008	9000	Repeated fracturing
Steady	2009-	13000	Maintain capacity, lower costs, enhancing oil recovery

The development roadmap of fracturing techniques in the Barnett shale gas reservoirs represents the progression of the recovery and the growing tendency of shale gas production in the world today.

2.3 Current research and application of fracture cleanup and choke size optimization

Shale gas production has drawn increasing attention due to the technical breakthrough of horizontal wells and multi-stage hydraulic fracturing. Both help unlock unconventional gas reservoirs (Zhang K. et al. 2015). Kaura, J.D. et al. (2001) stated that during hydraulic fracturing implementations, thousands of barrels of a fracturing fluid and tons of proppant materials are displaced as fractures are cleaning up. A discrepancy generally occurs between the expected fracture length and the effective production fracture length. Ayoub, J.A. et al, (2006) figured out that underperformance of hydraulic fractures is attributed to ineffective fracture cleanup. The post-fracking cleanup efficiency in shale gas formations has a remarkable effect on the long-term productivity of shale gas wells (Jamiolahmady, M. et al. 2007; Haidar, S. et al. 1996; Fossa, A. et al. 2007). Fracture cleanup efficiency is highly correlated with proppant volumes, multiphase flow, proppant crushing, polymer filter cakes and yield stress of concentrated gel in fractures (Wang, J. Y. et al. 2010; Mohan, J. et al. 2006).

Crafton and Gunderson (2007) illustrated that flowback of a fracturing fluid after multi-stage hydraulic fracturing of horizontal wells in shale gas reservoirs is a routine operation that influences the long-term production. Monifar et al. (2016) demonstrated that there is a large volume of the fracturing fluid that flows back during the fracture cleanup period. In field surveillances, cleats are created, which are filled with the

fracturing fluid. Flowback data is identified by the early time-pressure-rate (TPR) records. TPR is gathered immediately following the hydraulic fracturing of a well (Ilk et al, 2010). Recently, researchers (Williams-Kovacs and Clarkson, 2016) determined the potential to identify critical parameters, like fracture permeabilities and half-length, from the early-time production records. This information can have a significant impact on decision making. The flowback duration is usually short lasting only a few days. Based on historical production performance evaluation of shale gas wells, the parameters anticipated for the flowback data are normally identical to estimate long-term production performance. The ability to estimate the stimulation effectiveness while investigating the impact of two-phase flow in a rate transient analysis (RTA) is a significant finding.

Many researchers have investigated two-phase flowback performance and identified the fundamental fracture and reservoir data based on the production performance analysis over the long term. Ilk et al. (2010) proposed an extensive workflow for early-time flowback performance and discussed the flowback analysis and the interpretation of it. Clarkson and Williams-Kovacs (2013a; 2013b) conducted a quantitative interpretation for multi-phase flow of flowback performance to determine the critical fracture attributes. Flowing material balance (FMB) of multi-phase flow and type curves of shale gas production scenarios are utilized in their analytical patterns. However, the work is dependent on a coalbed methane recovery estimation model. Such models demand enhancing the Langmuir volume or integrating greater free gas contributions. They assume the water flowability in the matrix is negligible. The water is considered to originate from the cleats and gas from the adjoining matrix of the model. Adefidipe et al. (2014) and Xu et al. (2015) expressed a material balance equation

(MBE) methodology with a straight line for interpreting late-time gas production. They hypothesized that a fracture network is an open container with gas inflow from the adjacent matrix. The model failed to identify the crucial shale gas influx mechanisms: desorption, diffusion and slippage of gas and a non-Darcy flow effect. Ezulike et al. (2013; 2014) proposed a wholly analytical dual-porosity model with linear multi-phase flow based on the concept of dynamic relative permeability (DRP) for modeling late-time gas production performance in shale gas wells. There is a principal limitation; it does not explicitly model intricate fracture networks and the effect of gas desorption is neglected. Williams-Kovacs and Clarkson (2016) suggested a model that considers MBE by incorporating the linear transient flow of gas from matrix to cracks with multi-phase flow within the fracture networks. The influence of fracture geometry on the diagnosis graphs and gas diffusion were also not considered.

Maxwell et al. (2002) and Cipolla et al. (2008) identified that in shale reservoirs, a hydraulic fracturing treatment is generally accompanied with intricate fracture networks. Wu and Olson (2016) figured out that the complexity of fracture geometry is a product of the alternating actions between hydraulic fractures and intrinsic natural fractures. The emergence of an intricate fracture network is more common than primly predicted in unconventional formations (Olson 1995; Wu and Olson 2015). A considerable amount of work has been carried out on numerical, analytical and semianalytical methods with the intent to identify the well production performance in the intricate fracture networks. Dual porosity and dual permeability models (Warren and Root 1963; Blaskovich et al. 1983; Hill and Thomas 1985; Dean and Lo 1988), discrete fracture models (DFM) (Noorishad and Mehran 1982; Hui and Mallison 2009) and embedded discrete fracture

models (EDFM) (Li and Lee 2008; Moinfar 2014; Cavalcante et al. 2015) are utilized for simulating fluid flow in natural and/or induced fractured reservoirs in numerical approaches. These models fail to simulate the intricate fracture networks. DFM manages the intricate fracture networks but it is dependent on unstructured grids to align with the complexity of cracks. This is correlated with complicated gridding problems and costly computational endeavors. EDFM is a more effective model for fractured reservoirs because it can simulate long cracks and tiny fractures (which are handled implicitly). A preprocessing computer program is necessary to transfer the intricate natural/hydraulic fractures to a data array for a simulator. This creates a challenge for application because of the computational coding complexities. Zhou et al. (2014) suggested a semianalytical model that incorporates an analytical solution with a numerical reservoir simulation on the basis of discretized fracture segments. This model failed to contain the fundamental gas correctly conveying mechanisms of the shale gas formations. Yu et al. (2015) created an integrated semianalytical model that considers gas transport in shale reservoirs with complicated fracture width and conductivity, and diverse gas conveying mechanisms.

Holditch (1979) studied factors that influence water trapped in hydraulically fractured shale gas wells. He pointed out that reservoir parameters, like relative permeability, capillary pressure and hysteresis, play a significant role in identifying the cleanup performance. Tannich (1975) deduced that perpetual damage was impossible when the fracture conductivities were much higher than the formation conductivities. He described that one-half of the injected fracturing fluid would flow back to the surface within six days, if the gel in the fracturing fluid broke down adequately and the fracture

conductivity was great enough. This model did not consider capillary forces in the formation, closure-stress impacts, damage to cracks or the formation around the fractures. Lately, Gdanski et al. (2005) modeled the damages in the fracture faces and deduced that >90% of damages to fracture-face permeability can result in a significant enhancement of water production and a decrease in gas production. Cinco-Ley and Samaniego-V. (1981) suggested a relationship for evaluating the impacts of skin factors in fracture-face on well production performance. Lolon et al. (2003) investigated the influence of fracture conductivities on well production performance and stated that greater fracture conductivities could cause faster flowback of a fracturing fluid, longer efficient fracture length, and bigger cumulative gas production. May et al. (1997) investigated the influence of yield stress on the flowback of a fracturing fluid utilizing a numerical model. They deduced that increasing drawdown does not impact the volume of flowback. Improving the fracture conductivities does enhance the efficient fracture length. Yi (2004) developed a mathematical model and used a parametric analysis to investigate the influences of rheological properties and injection velocity. Friedel (2006) utilized a numerical reservoir model to research the impact of yield stress on the flowback of a fracturing fluid. He did not contrast this influence with other factors that impair the flowback of the fracturing fluid and gas productivity in shale gas wells. Typically, fracture damages are categorized as two types: damage inside fractures and damage in formation. Damage inside the fractures results from proppant crush and embedment. Damages in the fracture faces and fractures are blocked by chemicals or polymers. Cooke's (1975) work illustrated that the polymer residuals could be retained in the fractures. He reported excessive leakoff of a fracturing fluid, clay expansion,

relative permeability alteration and capillary effects that will normally result in damages inside the formation. Many other elements influence the cleanup procedure: a pressure drop, fracture geometry and conductivities, non-Darcy flow impacts, reservoir heterogeneities and temperature, viscosity of a fracturing fluid, viscous fingering, gel residuals, breaker and operational process.

Although poor proppant-carrying capacity is correlated with excessive water content in slick water (Fredd et al. 2001), a hydraulic fracturing treatment is low cost, and large-scale complex fracture networks can be created (Warpinski et al. 2005; Cipolla et al. 2009). Schein (2005) suggested the favorable aspects of hydraulic fracturing, like less reservoir damages and easier fracture cleanup. Palisch et al. (2008) depicted one concern about hydraulic fracturing. They found that a large portion of water injected during the course of treatment remains in the shale formation. In reality, millions of barrels of water are pumped into the target layer in multistage hydraulic fracturing stimulation of horizontal wells. It is common that only a small portion of injected water, normally 10 to 20%, can flow back to the surface during the flowback for fracture cleanup. The concern of industry was whether the lower fraction of water recovery would impair future gas production. The injected water trapped in the reservoir will raise water saturation and decline gas saturation, reducing gas mobility. The behavior of the trapped water will be governed by a variety of mechanisms, like imbibition controlled by capillary pressure, gravity segregation, relative permeability, and fracture conductivities with stress-sensitivity (Holditch 1979; Kamath and Laroche 2003; Gdanski et al. 2009; Mahadevan et al. 2009). When the remaining water is imbibed swiftly into the reservoir, it might not impact gas production. The fundamental issue to

study is to identify how unrecoverable water redistributes in hydraulic and induced fractures and matrix micropores in a reservoir.

Penny et al (2006), Mahadevan and Sharma (2003) acknowledged that injection of a fracturing fluid into a reservoir may result in reducing the absolute permeability. This is more likely to occur adjacent to the wellbore and fracture surfaces; the increasing water saturation causes a decrease in gas relative permeability. Penny et al (2006) determined the capillary pressure in diverse porous media. They illustrated that the capillary pressure in principal hydraulic fractures could be ignored. However, the capillary pressures in natural fractures and the matrix might be greater than several thousand psi. Alkouh et al (2013) combined this case study outcome with their simulation methodology. They used it to interpret the low recovery of injected water. He found that high capillary pressure could cause high water retention inside natural fractures. Relative permeability is normally regarded as another factor impacting water holdup in a reservoir. Some researchers have expressed that relative permeability in unconventional reservoirs may differ from that in conventional ones. Shanley et al. (2004) suggested a permeability jail in a relative permeability profile of shale gas formations, which is different from a conventional reservoir, and Blasingame (2008) stressed these properties of fluid flow in unconventional formations.

Imbibition is a significant factor affecting flowback, especially matrix imbibition. When the water is imbibed by the formation matrix, imbibition becomes an important mechanism retaining the water in the reservoir. The shale formation matrix is generally regarded as non-water wetting because it is the source of the hydrocarbon. Studies were conducted to determine whether the imbibition will occur and if so, whether it is

caused by natural fractures or by the matrix in shale reservoirs. Wang et al. (2012) studied the core samples from the Bakken Shale in North Dakota. They figured out that the shale is non-water-wetting. Dutta et al. (2012) investigated the fracturing fluid redistribution because X-ray computational tomography showed a spontaneous imbibition in hydraulically and naturally fractured reservoirs. After visualizing the water saturation distribution in the experimental core, the authors deduced that if the matrix was water wetting, some controlled imbibition occurs through the rock matrix thanks to the tiny pore throats and low permeability. They noticed that the leakoff of pumped water in shale reservoirs is associated with the incorporation of permeability, heterogeneity and a capillary effect. Makhanov et al. (2012) investigated the spontaneous imbibition of core samples from the Horn River Shale formation. They illustrated that the shale rock is able to suck in water and that the imbibition velocity is faster in a bedding orientation than when perpendicular to bedding direction. In their experiments, Odusina et al. (2011) and Wang et al. (2010) concluded that the imbibition is governed by fractures, instead of matrix. Roychaudhuri et al. (2011) identified imbibition dependent on mineral components in shale rocks: more clay and less total organic content resulted in more imbibition because water-wetting matters tend to inhale water. The imbibition of a shale reservoir is complicated because the inhomogeneous wettability system is extremely complex.

Mahadevan and Sharma (2003) announced that displacement and the subsequent vaporization are two flow regimes for the cleanup of water plugging. Zhang (2013) used this diagnostic approach to study the flowback mechanisms of shale gas wells in Barnett and Horn River Shale reservoirs. They noted flowback of fracturing in

Horn River Shale gas wells is governed by both mechanisms, but in Barnett Shale gas wells, flowback is controlled by displacement. Newsham et al. (2003) demonstrated that liquid phase vaporization in gas flow may cause extremely low water saturation, ultra-high capillary pressure and abnormal salinity increment. Rushing et al. (2008) stated that pressure, temperature and gas components are dominant factors impacting water dissolubility in gas. Sage and Lacey (1955) performed laboratory studies to determine the correlation between the vaporization ability and in-situ conditions with formation temperature and pressure.

Some researchers intended to simulate the flowback behavior in new models. Alkouh and Watternbarger (2013) developed a simulation model and stressed the significance of flowback records to PDA. They stated that an integrated permeability profile could be applied to simulate the flowback data. Clarkson (2012) created a method to estimate hydraulic fracture attributes with early-time flowback data. In his methodology, the flowback mechanisms of two-phase flow in a natural fracture system (cleats) are analogous to coalbed methane formations. Ezulike et al. (2013) proposed a flowback analytical model (FAM) by extending the linear dual-porosity flow model (DPM) to demonstrate flowback as a transient two-phase drainage process.

Munoz et al. (2009) stated that at the beginning of post-fracking production, the well performance principally correlates with fracture cleanup efficiency near the wellbore. The long-term well production forecasting, after fracturing, relates to cleanup in deep fracture faces. Crafton (2010) modeled the flowback and noticed that flowback behavior is associated with the water filling conditions in natural fractures. He identified that natural fractures are filled with gas or gas-rich liquid, a highly squeezable gas

bubble. Under high pressure, they will clean up the fractures as thoroughly as a water container. At the same time, he demonstrated that fractures filled with water have poor water displacement because of the lower compressibility and higher viscosity. A large pressure drop is necessary to cause gas coning into the bottom of fractures from the formation. The fracture conductivities are critical for the formation system and a flowback velocity is sensitive when gas goes into the fractures at the bottom of the reservoir.

Ehlig-Economides et al. (2012) illustrated that the future water production from a shale gas well could be affected by the hydraulic fracturing stimulation in an adjacent well. He demonstrated this influence in Horn River Shale wells. Zhang (2013) analyzed many Barnet Shale reservoir wells and determined that water production decreased when nearby wells had fracturing.

Crafton and Gunderson (2007) and Crafton (2008) pointed out that flowback of a fracturing fluid affected the future gas production performance. A high flowback velocity could be harmful to future production performance because proppant particles are moved back to the surface and consequently, fracture collapse might occur. Munoz et al (2009) stated that fracture cleanup impacts the original post-fracking gas production performance. The entire fracture face cleanup influences the future gas production performance over the long term. Cheng (2010) found shut-in impacted flowback behavior and gas production performance. After simulating gas wells in the Marcellus Shale reservoir, he noticed that when the post-fracking shut-in period is extended, gas production increases and the water production is reduced in comparison to shorter shut-in periods. He deduced that with capillary pressure, more water could be imbibed in the

matrix during the longer shut-in period. Ehlig-Economides and Economides (2011) suggested that the injected water might act as a proppant to maintain unpropped fractures open. They conclude that gas production performance in shale gas reservoirs with many wells is high when the volume of flowback of a fracturing fluid is very low.

The aforementioned researchers have studied the flowback behaviors in shale gas reservoirs in depth from many aspects, including water imbibition, two-phase flow, capillary pressure, complex fractures, relative permeability and fracturing fluid characteristics. Regrettably, adjusting a choke size dynamically according to wellhead pressure changing has seldom been considered in the literature, especially when the pressure in fractures is greater than the reservoir pressure. Jiang T. (2003) proposed a new analytical model of pressure drawdown under conditions of fracture closure. The model was based on the material balance theory and consequential fracture models (PKN and KGD) and the loss of the new extended fractures was a consideration too. Jiang T. (2008) built the optimization model for adjusting a choke size to post-fracking flowback of the material balance and fluid mechanics theories. He found the optimum choke size needs adjusting dynamically over time. It should consider the fracturing parameters, proppant precipitation distance and reservoir conditions in oil reservoirs. Hu J. (2008), Song W. (2013), Wen Q. (2009) and Wang et al. (2014) stated that models of forced fracture cleanup after hydraulic fracturing and the proppant backflow were based on the relative theories of material balance, rock and fluid mechanics. They described the migration model of proppant particles and identified the choke size and the closure time of hydraulic fractures. Zhang K. (2016) explored adjusting a choke size gradually by enlarging the diameter as fractures begin to close. However, none of these

researchers studied the influences of gas slippage effect and wellbore friction along the horizontal path on the wellhead pressure drop and choke size optimization.

2.4 Current commercial fracturing software

As mentioned before, there are lots of successful commercial software products available for hydraulic fracturing. They have many wonderful features and are successfully used by the oil and gas industry globally.

(1) GOHFER Grid Oriented Hydraulic Fracture Extension Replicator (http://barree.net/)

Developed by Barree & Associates LLC, this is a multi-disciplinary, comprehensive fracture simulator with geomechanics that integrates all the tools essential for well completion designs, analysis and optimization in both conventional and unconventional reservoirs. The features include a Planar 3D fracture simulator with a thoroughly incorporated fluid/solid transport model. It is used extensively for many formations, including shale reservoirs, naturally fractured formations and acid-fracking designs in carbonates.

(2) FracproPt (www.carboceramics.com/)

This tool by CARBO Ceramics Inc., is a design and analysis toolkit for hydraulic fracturing. It has powerful modeling abilities to estimate and determine the demanded perforation sections, the best fracture geometry and proppant conductivities. It can depict the proppant settlement, conductivity enhancements and fracture dimensions, and determine the impacts of proppant damages because of crushing, embedment, stress circulation, non-Darcy and multiphase flow. Its features involve evaluating stresses, permeability, pressures and other

rock properties, helping improve fracture design, and using for propped fracs, horizontal wells, foam fracs, acid fracs, frac packs and matrix acid. Reservoir properties can be directly imported from log files.

(3) Mangrove (www.slb.com)

It is developed by Schlumberger Ltd., and used for engineered stimulation design in the Petrel platform which is the only hydraulic fracturing simulator that integrates seamlessly with a comprehensive seismic-to-simulation work flow in both conventional and unconventional reservoirs. Stimulation design enables users to optimize production performance in shale reservoirs. Its features contain stimulation design, using reservoir properties for strategic staging and perforation selection and modeling both planar and nonplanar intricate fractures accurately. It considers vertical and lateral rock heterogeneities through 3D geological and geomechanical models. It is used for reservoir-, well- and completion-specific workflows, high-performance hydraulic fracture models, vertical, deviated and horizontal wells, and multistage completion designs.

(4)E-StimPlan (http://client.nsitech.com/StimPlan_Simulator/)

This is a complete and integrated simulator solution for stimulation design, analysis, and optimization developed by NSI Technologies LLC. It can optimize the well performance to reduce costs and decreasing environmental footprints, and has a comprehensive toolkit and the industry’s most viable geometry models. The user can use the models to increase production and decrease well costs by saving on proppant, pumping, and water disposal. The features include a range of fracture geometry simulation options available within StimPlan™ from

quick-look pseudo 3D methods to fully 3D gridded methods for more complicated problems, simulating multi-stage hydraulic fractures in horizontal wells, combining impacts of natural fractures, and visualizing microseismic events. It provides a solution for optimization of shale hydraulic fractures and real-time data acquisition.

(5) MFrac (https://www.bakerhughes.com/products-and-services/reservoir-development-services/reservoir-simulator/hydraulic-fracturing/mfrac-design-and-evaluation-simulator/)

It is a comprehensive suite of proven toolkits from Baker Hughes Inc. It covers a wide range of stimulation and petroleum engineering applications, including hydraulic fracturing, minifrac analysis, well production analysis, and real-time data acquisition. Mshale is a Natural Fracture Simulator, which contains a Discrete Fracture Network (DFN) simulator. The features include predicting fracture extension and degree of hydraulically fractured and naturally fractured reservoirs. It models multiple, cluster/complex/swarm and discrete fractures in shale and coalbed methane formations. The fracture characteristics, apertures, and propagation in three directions can be numerically simulated.

(6) FracMan (www.fracman.com)

Developed by FracMan Technology Group, this software has unique capabilities for the analysis and modelling of hydraulic fractures integrated with discrete fracture network modeling. It provides detailed analysis of the interaction of natural and hydraulic fractures, hydraulic fracture geometry and natural fracture reactivation.

Its features contain fracture modeling based on seismic attributes, geomechanical data and local features, such as folds, faults or stratigraphy. It can simulate well test matching for calibration of fracture aperture and permeability, upscaling fracture properties for full-field flow simulation, Monte Carlo simulation and uncertainty analysis.

Although there are many wonderful features in the abovementioned software, the disadvantages are evident. 1). Calculations are based on 3D models. It is very good to perform calculations with reservoir, fluid and fracture properties, but this is very complicated and time-consuming. 2). Fracture clean-up determines the well productivity after fracturing. It is not considered in the current simulator. 3). Professionals' intelligence is not fully utilized during the hydraulic fracturing design with the software.

Chapter 3 OPTIMIZATION OF CHOKE SIZE VS. WELLHEAD PRESSURE WITH TWO-PHASE FLOW

3.1 Introduction

After studying the flowback mechanisms and flow sequence and then deriving the equations for two-phase flow, this work focuses on building the optimization model for dynamic adjustment of a choke size as wellhead pressure changes over time. It uses a two-phase (gas and liquid) flow model along the horizontal, slanted and vertical sections. The forces acting on proppant particles, filtration loss of water, compressibility of a fracturing fluid, wellbore friction, a gas slippage effect, water absorption and adsorption are simultaneously considered in this model. The immovable fracturing fluid results from the fluid adsorption on fracture surfaces and the water absorption into clay material. A mathematical model is applied to characterize the fluid adsorption on the surfaces based on the Van der Waals force, electrostatic force and structural force. It quantifies the thickness of a water film. A theoretical model is used to describe the water absorption into the matrix's clay materials due to surface hydration and osmotic hydration. To determine the filtration loss of the fracturing fluid to the formation across the fracture faces, the formula to calculate the filtration velocity is identified by considering the fluid viscosity and the total compressibility of the formation fluid. In order to select the optimum choke size during the fracture cleanup, the wellhead pressure and choke size are varied over time to build a mathematical model using material balance, two-phase flow, rock mechanics and fluid mechanics. Compared with other traditional models, this model considers the forces acting on proppant particles, water loss, a gas

slippage effect, compressibility of the fracturing fluid, wellbore friction and the immovable fluid effect.

3.2 Surface Force and Water Adsorption

Shale gas is one of the unconventional gas resources, originating from organic substances in mudstone and kerogen via biogenic and/or thermogenic processes (Jarvie, D.M. et al. 2007). The water content in the micropores of shale rock under actual conditions influences the evaluation of gas deliverability. The apparent permeability (or a diffusion coefficient) decreases remarkably and the stress sensitivity of the shale matrix increases in the presence of adsorbed water (Pan Z. et al. 2010; Gensterblum Y. et al. 2014a; Gensterblum Y. et al. 2014b). The inorganic minerals of shale clay are constituted of three components: kaolinite, smectite and illite. They are always hydrophilic. The contact angles of shale clay are smaller than 60° via sessile drop tests, which results from the impact of minerals (Yuan W. et al. 2014; Dehghanpour H. 2012). Utilizing a NMRD technique, Korb et al. (2014) investigated sealed coring shale samples and figured out that water principally persists in the material pores. Ruppert et al. (2013) researched the accessibility of pores to methane and water through USANS/SANS diagnosis and illustrated that tiny pores (<30nm) were more accessible to water. In terms of the spontaneous imbibition experiments, the water uptake of intact shale samples was greater than the oil uptake (Xu M. et al. 2014; Dehghanpour H. 2013). At the same time, an extra driving force (disjoining pressure) resulted from material matter is also present when the water is being imbibed into shale pores (Binazadeh M. et al. 2015). The immovable water in a shale gas reservoir is classified as two types: (1) adsorbed water attached to a clay surface area and (2)

absorbed water trapped in a clay matrix network system (Hill H J. et al. 1979; Zhou M. 2000). Due to the Van der Waals force and the electric charge on clay surfaces, water molecules are strongly bound on the faces of clay particles or fractures by hydrogen bonds and an electrostatic force. In shale reservoirs, the adsorbed water on the clay surfaces can reach 2.63~7.19% of the total pore volume by a Tight Rock Analysis (TRA) (Boyer C. et al. 2006), and the immovable water cannot be negligible.

Jing Li et al. (2016) illustrated a quantitative description of water film thickness and distribution in shale clay minerals. This thesis focuses on analyzing the interaction between a solid phase (fracture surfaces), an immovable liquid phase (water film) and a movable liquid phase (fracturing fluid in fractures). The following assumptions are made: (1) fractures are filled with the fracturing fluid; (2) the inorganic fracture surfaces are strongly water-wet and occupied by water molecules (water film); (3) the water film is incompressible and homogeneous; (4) reservoir temperature maintains constant. In this study, disjoining pressure Π(h) suggested by B. V. Derjaguin et al. (1987) is implemented to illustrate the surface interactions between the solid phase, water film and movable liquid phase. Π*(h)* is disjoining pressure between the solid surface and the liquid film, which is related to the water film thickness and the relationship between surface forces and water film thickness. It is described as:

$$\Pi_{frac}(h) = \Pi_1(h) + \Pi_2(h) + \Pi_3(h) = -\frac{RT}{V_{mv}} \cdot \ln(RH) \qquad (3\text{-}1)$$

The total disjoining pressure is the sum of the London–Van der Waals force, Π_m, the electrical force, Π_e, and the structural force, Π_s (B. V. Derjaguin, 1987):

$$\Pi(h) = \Pi_m(h) + \Pi_e(h) + \Pi_s(h) \qquad (3\text{-}2)$$

where the London-Van der Waals force: $\Pi_m(h) = \frac{A_H}{h^3}$ (3-3)

Electrical force: $\Pi_e(h) = \frac{\varepsilon\varepsilon_0}{8\pi}\frac{(\zeta_1 - \zeta_2)^2}{h^2}$ (3-4)

And structural force: $\Pi_s(h) = ke^{-\frac{h}{\lambda}}$ (3-5)

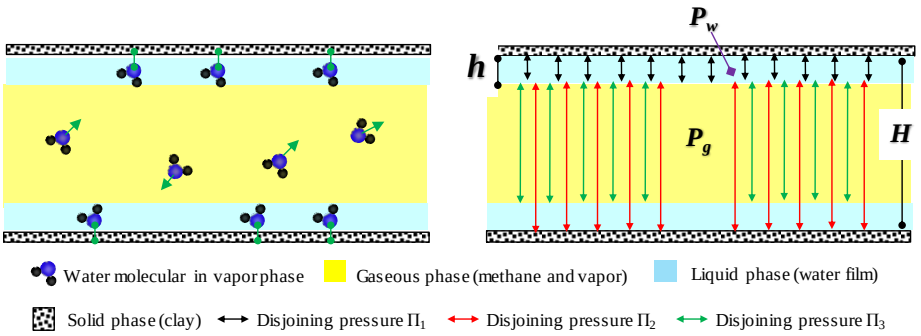

Figure 3-1 Mechanical equilibrium between solid phase, water film and movable liquid phase in hydraulic fractures (Jing Li et al 2016)

In Figure 3-1, the model of a hydraulic fracture is represented, where *H* is the width of the hydraulic fracture, which equals the diameter of a proppant particle, and *h* is the film thickness on the fracture surface. Except for the surface interaction $\Pi_1(h)$ between the water film and solid surface on which water is adsorbed, we also need to take $\Pi_2(h)$ and $\Pi_3(h)$ into account. These are interactions between the water film and its opposite surface, and interactions between two films adsorbed on the opposite walls, respectively.

$$\Pi_1(h) = \frac{A_H}{h^3} + \frac{\varepsilon\varepsilon_0}{8\pi}\frac{(\zeta_1 - \zeta_2)^2}{h^2} + ke^{-\frac{h}{\lambda}} \quad (3\text{-}6)$$

$$\Pi_2(h) = \frac{A_H}{(H-h)^3} + \frac{\varepsilon\varepsilon_0}{8\pi}\frac{(\zeta_1 - \zeta_2)^2}{(H-h)^2} \quad (3\text{-}7)$$

$$\Pi_3(h) = \frac{A_H{}^*}{(H-2h)^3} \quad (3\text{-}8)$$

In the research of Jing Li et al. (2016), Markus Tuller.et al. (1999) and Churaev et al. (2000), $\Pi_1(h)$ is the disjoining pressure between a water film and a solid surface on the same side considering both of the short-range (structural force Π_s) and long-range interactions (molecular force Π_m and electrical force Π_e), MPa; $\Pi_2(h)$ is the disjoining pressure between the water film and the surface on the opposite side, and we neglect short-range interactions (structural force Π_s) due to the relative long range between the film and its opposite fracture surface, MPa; $\Pi_3(h)$ is the disjoining pressure between two water films and only considers the molecular force Π_m because the potential difference between the two similar films is zero, MPa. In this study, V_{mv} is the molar volume of water, cm^3/mol; $RH=1.0$ is the water saturation in the hydraulic fractures, dimensionless; R is the gas constant, J/mol·K; T is the temperature, K; $A_H=1\times10^{-20}$J, is the Hamaker constant for solid-liquid interactions, J; $A_{H^*}=1.5\times10^{-21}$J, is the Hamaker constant for liquid-liquid interactions, J; $\varepsilon_0=8.85\times10^{-12}$F/m, is the electric constant in a vacuum; ε=81.5, is the relative dielectric permittivity of liquid, dimensionless; ζ_1 and ζ_2 are the electric potentials of the solid-water film and water film-movable fracture fluid interfaces, respectively, mV. An empirical value of $\Delta\zeta=\zeta_1-\zeta_2$=80Mv is adopted to depict clay/water film/movable liquid phase interactions when the condition of the contact angle is less than 60° (Churaev N. et al. 1995a; Churaev N. et al. 1995b); $k=1\times10^{-7}N/m^2$, is the coefficient for the strength of the structural force; λ=1.5nm is the characteristic length of water molecules (Churaev N. et al. 1995a; Churaev N. et al. 1995b).

3.3 Hydration Forces and Water Absorption

Water imbibition in shale has been discussed in several papers but only research with shale samples was considered. Odusina et al. (2011) carried out an experimental

study on a 1 inch × 1 inch core sample. However, only natural fractures were present in pores, meaning the imbibition effect was caused by the fractures, instead of the matrix, as shown in Figure 3-2. They deduced that Eagle Ford and Barnett tend to water imbibition. Wang et al. (2010) performed imbibition research on a thin shale outcrop core (1 to 5 mm). They described mineral dissolution (fractures) and crack due to clay swelling during the imbibition process.

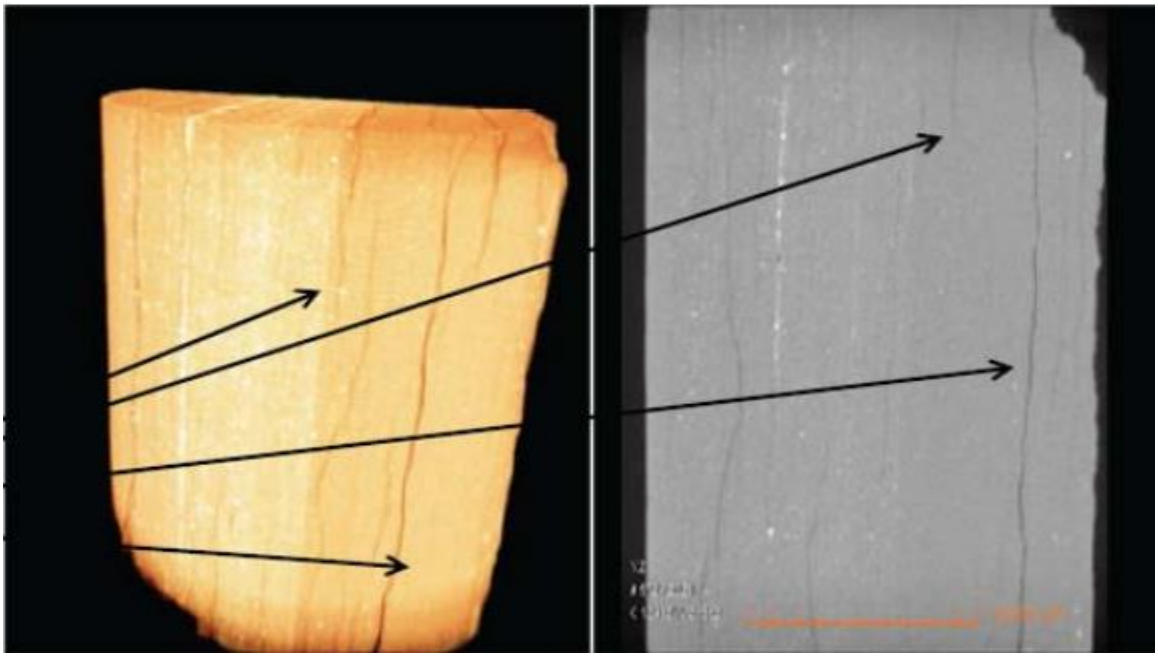

Figure 3-2 Image of Barnet shale samples showing the micro fractures with width around 0.00001 ft, Odusina et al. (2011).

Roychaudhuri et al. (2011) conducted water imbibition with shale samples and summarized that the percentage of both clay and organic matters have an influence on imbibition. If the samples had more clay and less total organic content (TOC), they prefer to imbibe more water and vice versa. This is because clay is generally water-wetting resulting in more water absorbed into the matrix surface. Shusheng Gao et al.

(2013) analyzed the shale components and water absorption due to the surface hydration and osmotic hydration. They determined water absorption after conducting SRV fracturing in a shale gas well based on the principle of equivalent network seepage capacity. They found that, if altering the fracturing fluid formula, the shale's water absorption would be impacted as well. Correspondingly, the flowback rate change.

3.3.1 Surface Hydration Force

Shale's surface hydration force is the water absorption potential energy resulting from deficiency of crystal water among clay lattices. More crystal water is lost as the reservoir temperature and pressure increase and the formation is deeper. The water absorption potential energy is greater and needs to absorb water molecules to recover equilibrium. Surface hydration can cause the interlayer space to be enlarged by four water molecules (about 1 nm) of thickness and twice the clay volume (Shusheng Gao et al.).

There is lots of clay in the shale formation, on whose surface a hydration effect occurs. When the fracturing fluid flows back, the pressure in the fracture network decreases and the water absorption potential energy increases so that the surface hydration enhances further, up to hundreds of Pa. As a result, a large volume of the fracturing fluid will not flow back.

3.3.2 Osmotic Hydration Force

Shale's osmotic hydration force is caused by the diffusion effect when there is a salinity difference between the formation water and fracturing fluid. The osmotic

pressure between two solutions with different salinity is described as (Shusheng Gao et al. 2013):

$$p = RT(\theta_{o1} m_1 e_1 - \theta_{o2} m_2 e_2) \quad (3\text{-}9)$$

where p is the osmotic pressure, atm (1 MPa = 9.8 atm); R is the gas constant; T is the absolute temperature, K; θ_o is the osmotic coefficient of saline solution; m is the salinity of solution; e is the number of ions in one mole of solvent.

Under the effect of the osmotic pressure, water molecules penetrate into the matrix continuously, causing further swelling of the clay. The swelling caused by the osmotic hydration can make the interlayer space to increase up to 12 nm. The osmotic hydration of shale results from the salinity difference between the original formation water and fracturing fluid. It causes the shale to absorb water and swell and the fractures become challenging to clean up.

3.3.3 Measuring the shale's water absorption velocity with experiments

Shusheng Gao et al. (2013) designed and performed experiments on water absorption in shale core samples, studying the water absorption capacity of the shale to distilled water, formation water and fracturing fluids. As shown in Figure 3-3, they proposed the experimental methods as follows: The core samples are trimmed as the slices, whose thickness is about 3.45 mm. The slices are cooling after they are heated with 100 °C for 48 hours. A shale core slice is suspended on the electric balance and it is immersed into the measured fluid. The weight of the slice is changing while the slice is absorbing water over time, which is recorded.

The measured fluids in the experiments are distilled water, formation water and fracturing fluids A and B, respectively. The water absorption velocity due to surface

hydration and osmotic hydration was identified, as shown in Figure 3-4. From Figure 3-4, the shale's water absorption capacity in distilled water is the maximum and the maximum water absorption is 0.0158 cm^3/cm^2. The second water absorption capacity is the one in formation water and the maximum water absorption is 0.0114 cm^3/cm^2. The water absorption capacity in fracturing fluid B is the weakest and the maximum water absorption is 0.009 cm^3/cm^2. The maximum water absorption capacity in fracturing fluid A is 0.0097 cm^3/cm^2.

Figure 3-3 Static water absorption experiments with shale core, Shusheng Gao et al. (2013)

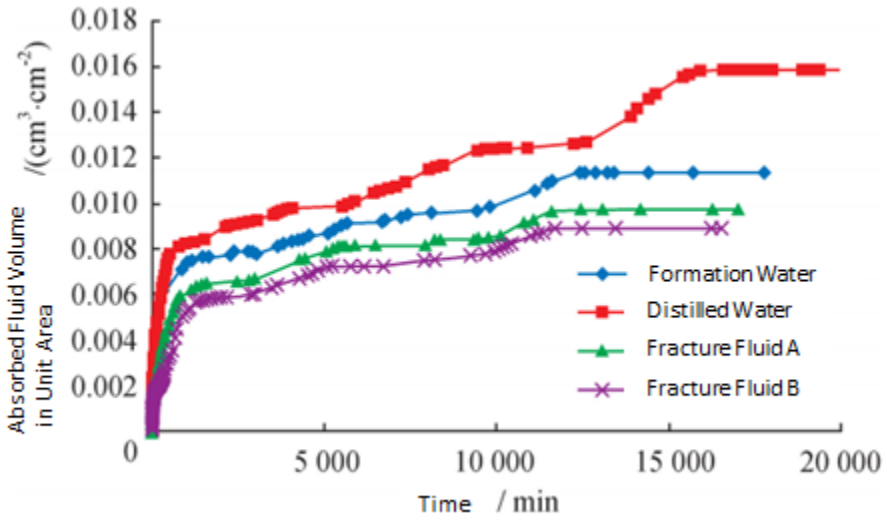

Figure 3-4 The graph of water absorption capacity of the shale core to diverse fluids, Shusheng Gao et.al (2013)

3.3.4 Estimating the water absorption volume

For shale gas, the prerequisite of effective development is large scale fracturing (volume fracturing) in a shale formation, which aims to obtain a complex fracture network and improve the osmosis capacity significantly. It is assumed that the fracture network (shown in Figure 3-5) is equivalent to the real fracture network in the shale reservoir after volume fracturing.

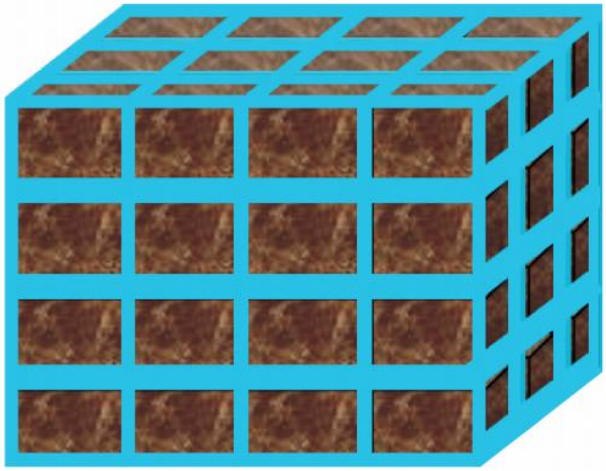

Figure 3-5 Equivalent fracture network of shale after volume fracturing, Shusheng Gao et al. (2013)

Shusheng Gao et al. (2013) stated that the fracture width is w (m). The length, width and height of a small shale cube are all a (m). Then, the surface area of the small shale cube is $S = 6a^2$ (m^2). The fracture volume controlled by each small shale cube is $V = 3a^2w$ (m^3). If the residual fracturing fluid in the wellbore is ignored, the water absorption ratio of each small shale cube is:

$$r_{wa} = \frac{6a^2 \cdot V_m \cdot \rho_f}{6a^2 \cdot V_m \cdot \rho_f + 3a^2 \cdot w \cdot \rho_f} = \frac{2 \cdot V_m}{2 \cdot V_m + w} \quad (3\text{-}10)$$

where r_{wa} is the water absorption ratio, dimensionless; ρ_f is the density of the fracturing fluid, g/cm^3; V_m is the maximum water absorption volume per unit area when the shale is immersed into the fracturing fluid during the course of experiments.

Using fracturing fluid A as an example, the maximum water absorption is 0.0097 cm^3/cm^2, while the fracture width is 0.2 mm and the water absorption ratio is 0.492. The fracture width is smaller than the water absorption surface area of the shale and the water absorption volume of the shale becomes larger as well. Hence, the result is more fracturing fluid cannot flow back.

3.4 Filtration loss velocity identification

Under high pressure, a fracturing fluid is injected into a horizontal section and the rock cracks if the pressure is greater than the breakdown pressure. The fracturing fluid with a greater injection pressure reopens existing micro-fractures. The fracturing fluid enters into those new fractures. Since the pressure in fractures is greater than the formation pressure, the fracturing fluid permeates into the formation across the fracture faces. The invaded zones against the fracture faces come to play as shown in Figure 3-6. Panga et al. (2007) stated that in shale formations, water blocking generally happens near the wellbore and fracture faces. Penny et al. (2006) determined that about 60% to 90% of fracturing fluids are trapped near the fracture zones in Barnett Shale gas formations. King (2010), Warpinski et al. (2008) and Cipolla et al. (2008) described a created fracture network or fracture complexity in some shale formations and the existing natural fractures or induced fractures as orthogonal to the principal fractures where fracturing fluids are trapped. Ehlig-Economides and Economides (2012) discussed the distribution of the water in a stimulated reservoir volume, and illustrated that the water in either propped hydraulic fractures or in unpropped natural fractures could be simulated. Apiwathanasorn and Ehlig-Economides (2012) verified that micro-fractures were reopened through a production performance analysis of hydraulically fractured shale gas wells in the Barnett Shale. Fan et al. (2010) reported that the majority of a fracturing fluid is absorbed into shale matrix or a fracture system, in complex fracture networks or planar fractures. In order to study the imbibition of water into the shale core, Odusina et al (2011) conducted experiments to illustrate the imbibition effect is due to micro-fractures and the matrix. Wang et al. (2010) carried out

the core experiments and demonstrated that fractures and matrix influence imbibition. Alkouh and Watternbarger (2013) calculated the ratio of lost water in a reservoir by adjusting 20% flowback efficiency and determined that 50% of the total fracturing fluid is lost to some locations that do not efficiently communicate with the flow path to a well.

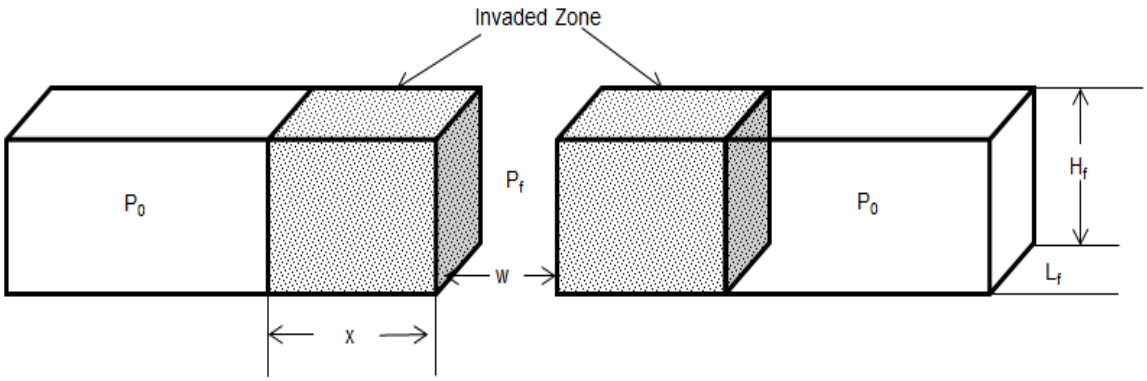

Figure 3-6 Filtration loss zone distribution graph

This work indicates that the fracturing fluid permeating into the formation is governed by two natural mechanisms: 1) the viscosity of the fracturing fluid and 2) the total compressibility of formation fluids. The filtration loss of a fracturing fluid volume is usually represented by a filtration loss coefficient.

3.4.1 Filtration loss velocity controlled by the viscosity of fracturing fluid (Wang, H. et al. 1998)

It is assumed that the fracturing fluid permeates into a formation perpendicular to fracture faces. The filtration loss velocity can be derived with Darcy's law:

$$v_{fl1} = 0.058 \cdot \frac{K \cdot \Delta P_1}{\mu \cdot x_L} \tag{3-11}$$

where v_{fl1} is the filtration loss velocity controlled by the viscosity of the fracturing fluid, m/min; K is the formation permeability μm^2; ΔP1 is the pressure difference that causes the filtration loss controlled by the viscosity of fracturing fluid, MPa; μ is the apparent

viscosity of the fracturing fluid in the fractures under the condition of flowing, mPa.s; x_L is the filtration distance from the fracture face, m.

Generally, the actual filtration loss velocity of the fracturing fluid is:

$$v_a = 0.058 \cdot \frac{K \cdot \Delta P_1}{\mu \cdot \emptyset \cdot x_L} \tag{3-12}$$

where Ø is the formation porosity, fraction.

Since $v_a = \frac{dx_L}{dt}$, $\int_0^{x_L} x_L \cdot dx_L = \int_0^t 0.058 \cdot \frac{K \cdot \Delta P_1}{\mu \cdot x_L} \cdot dt$, the x_L can be solved through the integration of the above equation, resulting in:

$$v_{fl1} = 0.058 \cdot \frac{K \cdot \Delta P_1}{\mu \cdot \left(\frac{0.116 \cdot K \cdot \Delta P_1 \cdot t}{\mu \cdot \emptyset}\right)^{\frac{1}{2}}} = 0.17 \cdot \left(\frac{K \cdot \Delta P_1 \cdot \emptyset}{\mu \cdot t}\right)^{1/2} \tag{3-13}$$

Thus, we can get the pressure difference which causes the filtration loss controlled by the viscosity of the fracturing fluid, ΔP_1:

$$\Delta P_1 = \frac{v_{fl1}^2}{0.0289} \cdot \frac{\mu \cdot t}{K \cdot \emptyset} \tag{3-14}$$

3.4.2 Filtration loss velocity controlled by total compressibility of formation fluid (Wang, H. et al. 1998)

Any unit volume is selected in the formation. If the rock expansion is neglected, the fluid volume in the unit formation volume is: $\bar{V} = A \cdot \emptyset \cdot dx$ (3-15)

Since the pressure drop is dP, the fluid volume enlarges by:

$$d\bar{V} = C_f \cdot \bar{V} \cdot dP \tag{3-16}$$

where C_f is the compressibility coefficient of the fluids, including gas and liquid, MPa^{-1}; Substitute $\bar{V}$ in eq.(3-16) into eq. (3-15), and differentiate it. It is written as:

$$\frac{\partial q}{\partial x} \cdot \frac{\partial q}{\partial x} = -A \cdot \emptyset \cdot C_f \cdot \frac{\partial P}{\partial t} \tag{3-17}$$

The linear Darcy's percolation law is: $q = -0.058 \cdot \frac{K \cdot A}{\mu} \cdot \frac{\partial P}{\partial x}$ (3-18)

In x, it is differentiated: $\frac{\partial P}{\partial x} = -0.058 \cdot \frac{K \cdot A}{\mu} \cdot \frac{\partial^2 P}{\partial x^2} = -A \cdot \emptyset \cdot C_f \cdot \frac{\partial P}{\partial t}$.

The formula above is a linear diffusion equation and the Laplace transform can be used to solve the solution:

$$\frac{P(x,t)-P_R}{\Delta P_2} = erfc\left(\frac{x}{2 \cdot \sqrt{\pi \cdot t}}\right) \quad (3\text{-}19)$$

where P(x,t) is the pressure at any time t and at any place x in the formation, MPa; P_R is the formation pressure, MPa; ΔP_2 is the pressure difference which causes the filtration loss controlled by the total compressibility of the formation fluid, MPa. Erfc() is the Gauss Error Function.

The filtration loss velocity at fracture faces is:

$$v_{fl2(x=0)} = -0.058 \cdot \frac{K}{\mu} \cdot \left(\frac{\partial P}{\partial x}\right)_{x=0} \quad (3\text{-}20)$$

Differentiate in x in eq.(3-19): $\left(\frac{\partial P}{\partial x}\right)_{x=0} = -\frac{\Delta P_2}{\sqrt{\pi \cdot t \cdot \frac{0.058 \cdot K}{\mu \cdot \emptyset \cdot C_f}}}$ (3-21)

Substitute eq.(3-21) into eq. (3-20): $v_{fl2(x=0)} = -0.058 \cdot \frac{K}{\mu} \cdot \frac{\Delta P_2}{\sqrt{\pi \cdot t \cdot \frac{0.058 \cdot K}{\mu \cdot \emptyset \cdot C_f}}}$ (3-22)

So $v_{fl2(x=0)} = 0.136 \cdot \Delta P_2 \cdot \left(\frac{K \cdot C_f \cdot \emptyset}{\mu \cdot t}\right)^{1/2}$; that is

$$\Rightarrow \Delta P_2 = \frac{v_{fl2}}{0.136} \cdot \left(\frac{\mu \cdot t}{K \cdot C_f \cdot \emptyset}\right)^{1/2} \quad (3\text{-}23)$$

The total filtration loss velocity of the fracturing fluid, caused by both the viscosity of the fracturing fluid and the compressibility of the formation fluid is:

$$v_{flt} = v_{fl1} + v_{fl2} = 0.17 \cdot \left(\frac{K \cdot \Delta P_1 \cdot \emptyset}{\mu \cdot t}\right)^{1/2} + 0.136 \cdot \Delta P_2 \cdot \left(\frac{K \cdot C_f \cdot \emptyset}{\mu \cdot t}\right)^{1/2} \quad (3\text{-}24)$$

3.5 Threshold velocity of proppant particle start-up

During hydraulic fracturing operations in shale gas reservoirs, slick water is used as the fracturing fluid because it has low viscosity and weak sand carrying capacity. The proppant particles in the slick water settle at the bottom of fractures immediately after the pump stops. The proppant particles are cohesive to each other and the cohesion forces occur between the particles. Choi S. et al. (2001) studied and acknowledged the lifting mode is relevant to both bedload and suspended load. They gave a descriptive formula for a lifting force analysis when the particles start lifting up. Zhang K. et al. (2016) revealed that when proppants flow in a transverse fracture in a horizontal well, lifting can cause the proppants to flow back to the surface. When applying the lifting mode, the mechanics analysis is conducted for a single particle, as shown in Figure 3-7. The mechanics balance equation, under the threshold conditions of proppant particles start-up, can be achieved. The calculation model of the threshold velocity of a particle during fracturing fluid flowback in shale gas reservoirs can be derived.

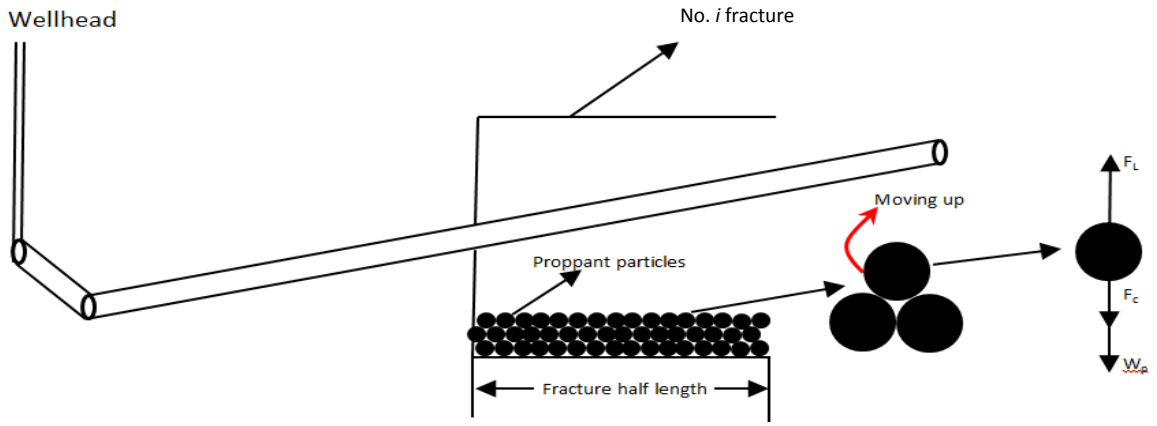

Figure 3-7. The start-up model and mechanics analysis for flow-back of proppant particles in No. *i* fracture

In the lifting mode, the threshold condition for the particle to be picked up by the flow takes place when the lifting force equals the sum of the submerged weight of the particle and the equivalent cohesion forces among particles:

$$F_l = W_o + Fc \tag{3-25}$$

The submerged weight of the particle is given by:

$$W_o = \frac{\pi}{6} \cdot d_s^3 \cdot g \cdot (\rho_s - \rho_f) \tag{3-26}$$

The cohesion forces among particles are:

$$F_c = \frac{\pi}{32} \cdot d_s \cdot \varepsilon_c \tag{3-27}$$

The non-uniformity of magnitude of the fluid velocity acting on the particle results in the top and the bottom, respectively, and the lifting force acts vertically upward. The lifting force Fl can be expressed as:

$$F_l = C_l \cdot \frac{\pi \cdot d_s^2}{4} \cdot \frac{\rho_f \cdot u_B^2}{2} \tag{3-28}$$

The threshold velocity of the proppant particle start-up is:

$$u_B = 2 \cdot \sqrt{\left(\frac{d_s^2 \cdot g}{3} \cdot (\rho_s - \rho_f) + \frac{\varepsilon_c}{16}\right) \Big/ (C_l \cdot d_s \cdot \rho_f)} \quad (3\text{-}29)$$

where u_B is the threshold velocity of the proppant particle start-up, m/sec; F_l is the lifting force acting on the particle, N; Fc is the cohesion force acting on the particle, N; Wo is the submerged weight of the particle, N; C_l is a lifting force coefficient, dimensionless; ρ_f is the fracturing fluid density, kg/m^3; ρ_s is the proppant particle density, kg/m^3; d_s is the proppant particle diameter, m; g is gravitational acceleration, 9.80665 m/s^2; ε_c is a cohesion force coefficient among particles, 0.00256 N/m.

3.6 Gas releasing velocity from fracture faces when pressure in fractures is larger than formation pressure

3.6.1 Theoretical background

Shale rock contains complex ingredients, including clay minerals, silica minerals, carbonate minerals and organic matters (Fu X. et al. 2011; Nie H. et al. 2012; Liu H. et al. 2009). Normally, clay and silica minerals are water-wetting, while carbonate minerals and organic matters are non-water-wetting. A shale gas reservoir includes approximately 2-25% organic materials. Curtis J. B. (2002) described natural gas in shale reservoirs stored as free gas in both mineral pores and natural fractures. A large portion of gas is adsorbed on shale faces and the adsorbed gas generally ranges from 20-80%. Ross et al. (2009) determined that the adsorbed gas is stored in microporous and mesoporous domains of the organic matters and clay minerals. Clay is the principal component of mud shale and it is widely distributed in a reservoir. It has a unique crystal

structure and properties. The fundamental minerals found in clay are kaolinite, illite, chlorite and montmorillonite (Zou C. et al. 2013).

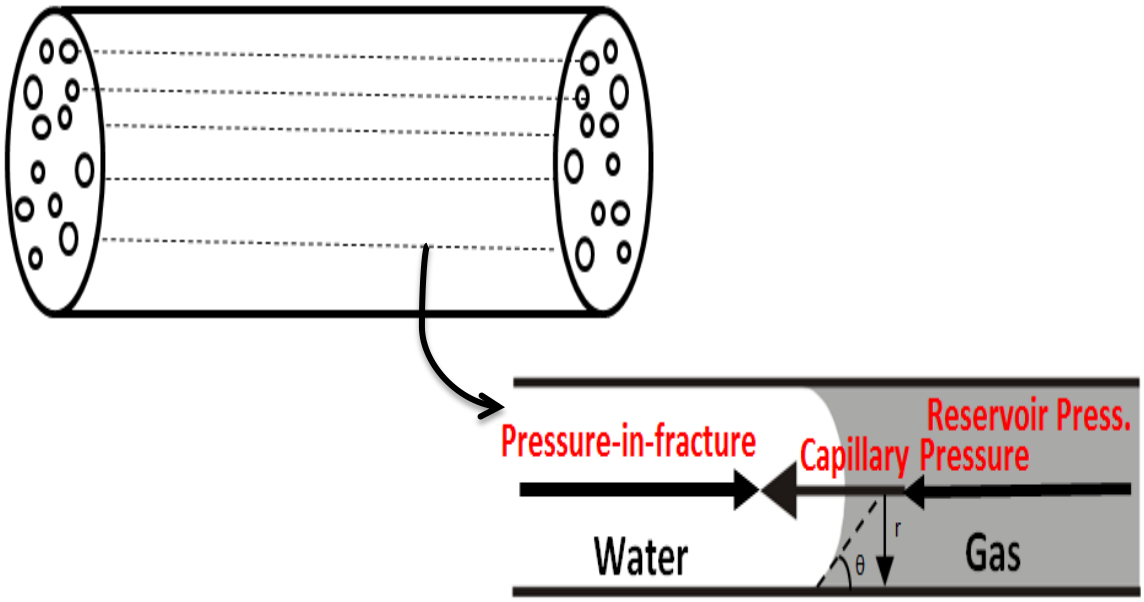

Figure 3-8 Hypothesis picture of shale pore structure and the gas plug is acted by the forces of pressure in fractures, reservoir pressure and capillary pressure

After shale rock is cracked, the water in the fracturing fluid enters into the reservoir. Clay minerals are water-wetting and tend to adsorb water molecules. The water molecules take the spots of gas molecules on the surfaces of clay minerals and the gas is releasing. This procedure is called substitution. The released gas joins with other free gases, existing in mineral pores and natural micro-fractures. Under high pressure in fractures after hydraulic fracturing, the water tries to permeate into the porous media. The gas plug is acted on by the force of the pressure in fractures, reservoir pressure and capillary pressure. It is assumed that the hypothesized system is horizontal and the gravitation is neglected, as shown in Figure 3-8.

Penny et al. (2006) identified that shale core capillary pressure can be as high as 2000 psi when the pore size is extremely tiny. A fracture width is very large in hydraulic fractures, and capillary pressure is very small and negligible. However, in natural fractures and matrix, capillary pressure is the important force to imbibe water into the matrix and then to hold water in the natural fractures. If the gas plug is situated within a section of organic matter or carbonate minerals (non-water-wetting), the capillary pressure becomes the driving force to move the gas plug. The goal of this work was to analyze the forces that act on it quantitatively, and then try to calculate the range of capillary pressure. Gao S. et al. (2004) recognized that the pore structures in real rock are extremely complicated and there are not diameter-equal round throats, which are simply straight and smooth. If any tiny section of a pore throat is selected, it can be regarded as a straight, smooth and round capillary.

Green D.P. et al. (2008) presented the formula of capillary pressure:

$$P_{cap} = -\frac{2 \cdot \sigma \cdot cos\theta_{cap}}{r} \tag{3-30}$$

where P_{cap} is capillary pressure, MPa; σ is the surface tension of water and gas, N/m; θ_{cap} is contact angle among water, gas and rock, dimensionless; r is the radius of the selected section of capillary throat, m; negative sign (-) means the direction of capillary pressure is opposite to the direction of water flow.

Glover P. (2010) stated the range of contact angels in the table below:

Table 3-1 Contact angles for different wettabilities. (Glover P. 2010)

Contact Angle relative to water, θ_{cap} (degrees)	Description
0	Extremely water wet
0-30	Significantly water wet
30-60	Moderately water wet
60-90	Weakly water wet
90	Neutrally wet
90-120	Weakly non-water wet
120-150	Moderately non-water wet
150-180	Significantly non-water wet
180	Extremely non-water wet

Vargaftik N. B. et al. (1983) presented a table, which demonstrated the surface tension of water and gas as a function of temperature. The tension ranges from 72.75 – 50.85 $\times 10^{-3}$ N/m if the experimental temperatures are from 20 – 140°C.

Nelson P. (2009) illustrated that the pore-throat diameters in shales range from 0.005 – 0.116 μm.

With the abovementioned data, the range of capillary pressure can be calculated. Under 20°C, it ranges 0 - 58.2 MPa; under 140°C , it is from 0 – 40.68 MPa.

Assume that the pressure in fractures is about 20MPa greater than the reservoir pressure. It is plausible that the gas plug can move into hydraulic fractures with the action of the capillary force. When the gas goes into the hydraulic fractures, the gravitational segregation occurs. The gas density is much lower than the fracturing fluid density; gas goes up and enters into the wellbore. It is produced along with the flowback toward the surface.

3.6.2 Gaining gas releasing velocity from field production tests and surveillance

It is noted that the gas releasing velocity came from shale surfaces via the field production tests and surveillance. Kanfar M. (2017) provided an example with a liquid-rich shale well from the Montney formation, as shown in Figure 3-9. The targeted reservoir has a thickness of 200 ft and a total porosity of 6%. This well is horizontally drilled and hydraulically fractured in nine stages. The average stage spacing is around 760 ft apart, and they are stimulated with two perforation clusters. After hydraulic fracturing, the well carried out flowback for 10 days, shut-in for 73 days, and then was opened for production to sales lines.

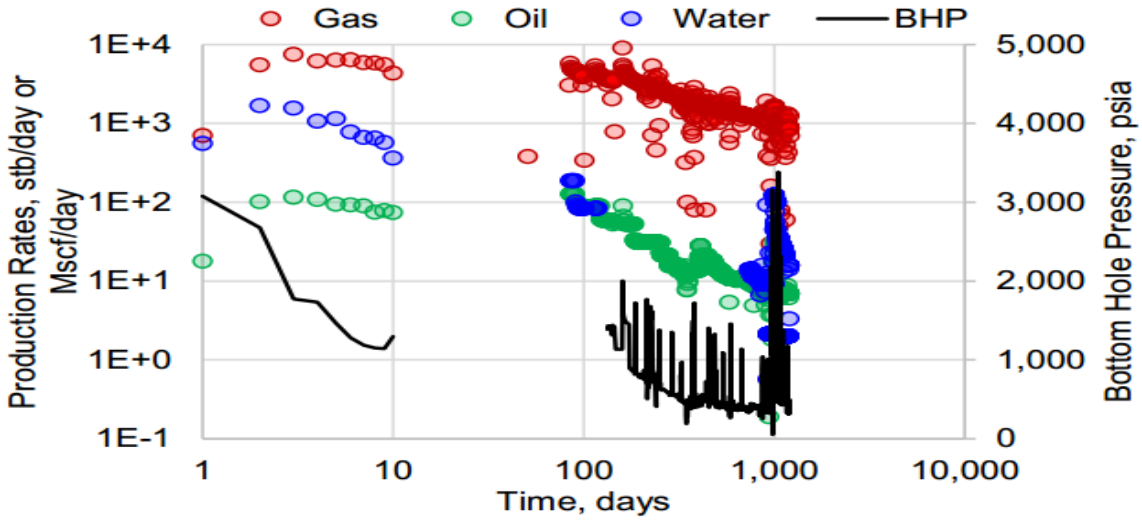

Figure 3-9 Flowback and production data of a well from Montney Formation, North America (Kanfar M. 2017)

3.7 Modeling pressure drop with two-phase flow along the wellbore and choke size optimization

In order to model the pressure drop along the wellbore and choke size optimization as precisely as possible, flow phenomenon was divided into two scenarios.

One is pure liquid flow and the other is two-phase (gas and liquid) flow. The assumptions are:

1) Flow patterns are out of consideration in this work;
2) During the two-phase flow, there is a uniform distribution of gas and a fracturing fluid in any tiny unit volume along the wellbore, and only the percentage of gas and the fracturing fluid changes when the temperature and pressure are altering;
3) Along with the horizontal section of the wellbore, the temperatures are same at any point;
4) All proppant particles are spherical and identical in shape and size;
5) Natural gas is releasing from each hydraulic fracture at every specific time interval.
6) After the flowback begins, the fractures start closing. The heights and lengths of fractures are unchanged during fracture closure, and only the widths decrease.
7) When the fluid is flowing through the wellbore, the energy loss to the environment is neglected.

According to the theories of material balance and volume balance, during the period of fracturing fluid flowback, the fractures volume alteration equals the sum of filtration loss volume, flowback volume, the volume of water adsorption and absorption of the fracturing fluid. The fractures volume alteration is proportional to $(1-\gamma^2)/E$, where γ is the shale's Possion's ratio (dimensionless) and E is Young's Modulus (MPa).

3.7.1 Pure liquid flow

During the course of pure liquid flow, the model is built to optimize the choke size and calculate the pressure drop along horizontal, slanted and vertical sections of wellbore, respectively (shown in Figure 3-10).

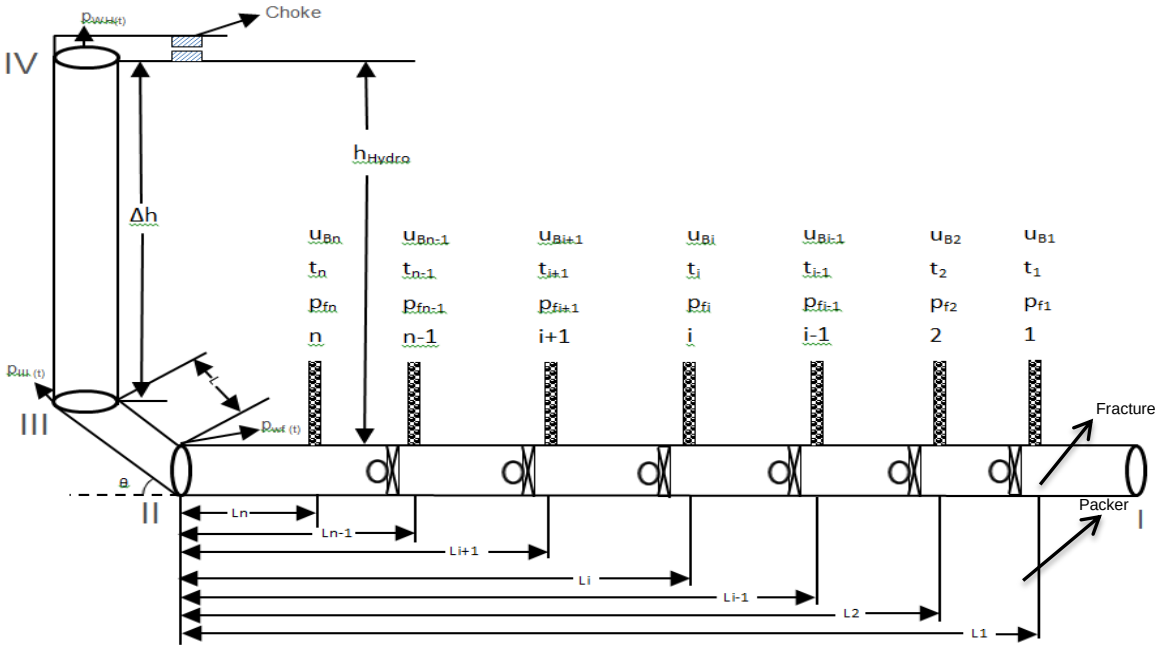

Figure 3-10 Scheme picture of pure liquid flow scenario along the wellbore

1) Flowing along the horizontal path

At the beginning of flowback, it is the pure liquid flow in the fractures and wellbore without gas. Colebrook C.F. (1933) suggested a formula to calculate the pressure drop along the horizontal pipe considering the roughness. According to the theories of material balance and volume equilibrium, during the course of fracture closing, the altering volume of fractures is equal to the sum of the filtration loss volume, water adsorption and absorption and flowback volume.

The maximum velocity of liquid flow is u_B (threshold condition) and the volume flow is: $Q_L = u_B \cdot \frac{\pi \cdot d^2}{4}$, where Q_L is the volume flow of pure liquid flow, m^3/sec; d is the diameter of wellbore, m.

The Reynolds number can be calculated with the formula (Moody L.F. 1944):

$$R_e = d \cdot u_B \cdot \rho_f / \mu_l \tag{3-31}$$

where Re is the Reynolds number, dimensionless; ρ_f is the density of the fracturing fluid, kg/m^3; μ_l is the viscosity of the fracturing fluid, mPa.s.

The friction resistance coefficient along the horizontal path can be illustrated as (Bertuzzi A.F. 1956):

$$\lambda = 0.0056 + \frac{0.5}{R_e^{0.85}} \tag{3-32}$$

The pressure drop along the horizontal section can be described as:

$$P_2 - P_1 = \left(\lambda \cdot \frac{1}{d} \cdot \frac{u_B^2}{2} \cdot \rho_f\right) \cdot \Delta L \tag{3-33}$$

where P2 is the pressure at the end point of the horizontal section, MPa; P1 is the pressure at the point of the first stage of a hydraulic facture, MPa; ΔL is the length of the horizontal section of wellbore, m.

2) Flowing along the slanted section

Flanigan O. (1958) suggested that the pressure drop along the slanted section is the sum of the pressure reductions caused by both a height difference and friction loss along the slanted path. The calculation formula is:

$$P_{wf(t)} - P_{III(t)} = \rho_f \cdot g \cdot LS \cdot sin\theta + \left(\lambda \cdot \frac{1}{d} \cdot \frac{u_B^2}{2} \cdot \rho_f\right) \cdot LS \tag{3-34}$$

where $P_{wf(t)}$ is the pressure at the end point of the horizontal section at any time t, MPa; $P_{III(t)}$ is the pressure at the end point of the slanted section at any time t, MPa; LS is the length of the slanted path, m; θ is the angle between the horizontal and slanted sections, dimensionless.

3) Flowing along the vertical path

Moody L. F. (1944) demonstrated the equations to calculate the friction factors and pressure drop in vertical pipe flow. When the fluid is flowing along the vertical section from bottom to top if it is the pure liquid flow, it supposes that it does not work to the environment outside so that there is no energy loss. The cross-sectional area vertically along the wellbore remains unchanged. When flowing from bottom to top along the wellbore, the total dynamic fluid height can be considered as a calculation analogous to Darcy's law. The pressure drop along the vertical section can be described as:

$$P_{III(t)} - P_{wh(t)} = \rho_f \cdot g \cdot \Delta h \cdot (1 + \frac{\lambda \cdot u_B^2}{2 \cdot g \cdot d}) \quad (3\text{-}35)$$

where $P_{wh(t)}$ is the wellhead pressure at any time t, MPa; $P_{III(t)}$ is the pressure at the end point of the slanted section at any time t, MPa; Δh is the height of vertical path of the wellbore, m.

4) Flowing through a choke

Flowing through a choke from the wellhead can be illustrated with Bernoulli's equation (Hu J. et al. 2008):

$$\frac{P_{wh(t)}}{\rho_l} + \frac{u_B^2}{2} = \frac{P_0}{\rho_l} + \frac{v_c^2}{2} + \xi \cdot \frac{v_c^2}{2} \quad (3\text{-}36)$$

where P_0 is the setup pressure at the outlet of the choke, MPa; v_c is the flow velocity at the outlet of the choke, m/sec; ξ is the local resistance coefficient when the fluid is flowing through the choke, dimensionless.

Using the continuity equation: $u_B \cdot \frac{\pi \cdot d^2}{4} = v_c \cdot \frac{\pi \cdot d_c^2}{4}$, where d_c is the choke diameter, m. The pressure drop flowing the choke can be demonstrated as:

$$P_{wh(t)} = P_0 - \frac{\rho_f}{2} \cdot u_B^2 + \frac{1+\xi}{2} \cdot u_B^2 \cdot \frac{d^4}{d_c^4} \quad (3\text{-}37)$$

Solving these equations simultaneously, the relationship curve is achieved using $P_{wh(t)}$ vs. d_c. This means the choke size can be adjusted dynamically according to the wellhead pressure alteration over time.

3.7.2 Two-phase flow (gas and liquid)

In terms of field production tests and surveillance, gas releases after a specific time. When the gas flow occurs, it becomes two-phase flow (gas and liquid). During the course of two-phase flow, the model is built to optimize the choke size and calculate the pressure drop along horizontal, slanted and vertical sections of wellbore, respectively (shown in Figure 3-11).

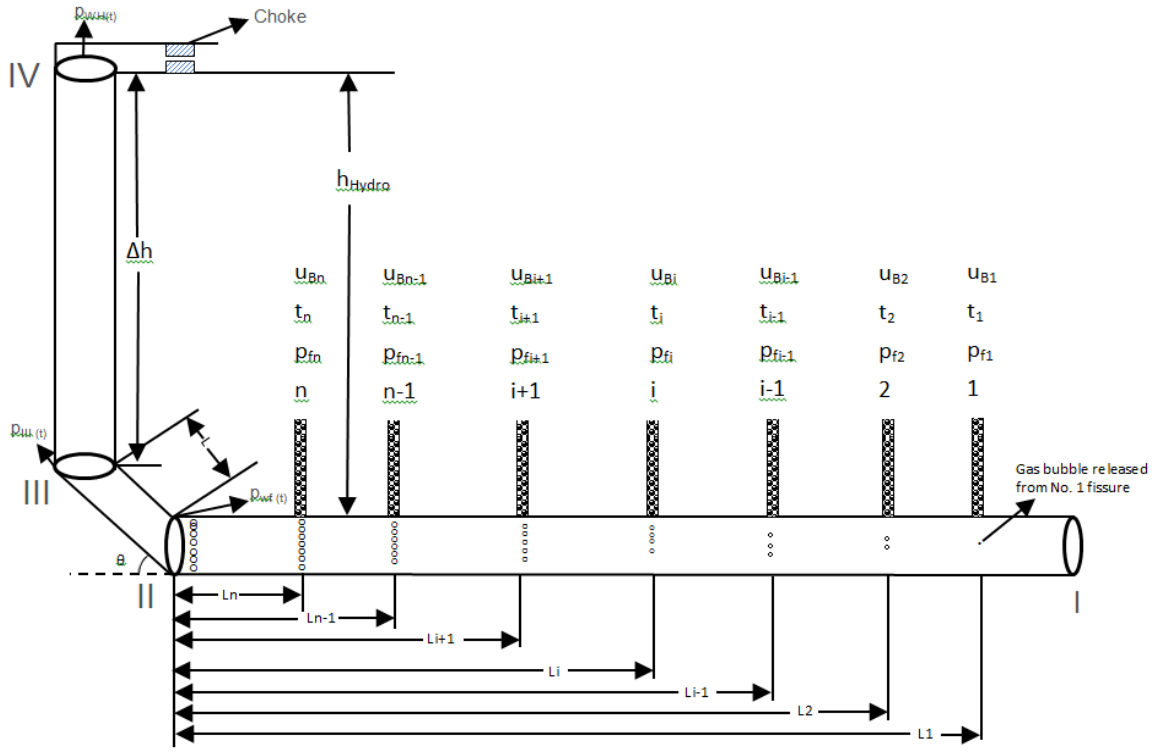

Figure 3-11 Scheme picture of two-phase flow (gas and liquid) scenario along the wellbore

1) Gas slippage effect during two-phase flow

Chen J. (1988) stated that slippage is a phenomenon in which natural gas is passing by the liquid in the two-phase (gas and liquid) flow, caused by the temperature and/or pressure changing. When flowing through a pipe, the gas characteristics are different from those of the liquid. The gas cannot form a thin adsorption film on the pipe wall. The flowing velocity of gas molecules at the pipe center is almost identical to that of those at the pipe wall. This property is called the ‘gas slippage effect’. During two-phase flow, the gas always moves faster than the liquid. That variation causes a density change to the mixture in the pipe. The mixture density at the forefront part is usually larger than the density at the back where the slippage phenomenon occurs. There is an

additional pressure loss to maintain the two-phase flow continuously, as shown in Figure 3-12.

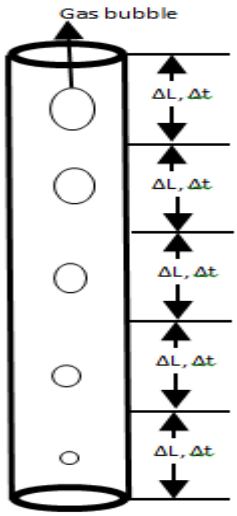

Figure 3-12 Scheme picture of a gas slippage effect in two-phase flow (gas and liquid) scenario

2) Flowing along the horizontal path during two-phase flow

Bertuzzi A.F. (1956) developed a methodology to analyze the simultaneous flow of gas and liquid through a horizontal pipe.

It is an assumption that when fractures close, the fracturing fluid is flowing back at a maximum velocity.

Assume that a tiny section of the wellbore is selected (dL >0). In the cross section of passage, gas and the fracturing fluid distribute evenly. The pressure is P and the temperature is T. This is an isothermal process as the mixture of gas and liquid flow along the horizontal wellbore. Under the conditions of P and T, the compressibility coefficient of natural gas is Z(P).

From the production tests and surveillance, after a specific time tg, gas releases due to capillary pressure and substitution even though the pressure in fractures is greater than reservoir pressure.

At time t >tg, at the point of No. *i* fracture, the gas flow rate in the wellbore is:

$$Q_{ri}(t) = 4 \cdot v_r(t) \cdot L_{fi} \cdot H_{fi} \cdot (t - t_g) \quad (3\text{-}38)$$

where $Q_{ri}(t)$ is the gas flow rate at time t at the point of No. *i* fracture in the wellbore, m^3/sec; $v_r(t)$ is the velocity of the gas releasing from shale face at time t, $m^3/(m^2.sec)$; L_{fi} is the half length of No. *i* fracture, m; H_{fi} is the height of No. *i* fracture, m; tg is the specific time when the gas starts releasing from shale faces, s.

The true gas content $x_i(t)$ at the point of No. *i* fracture in the wellbore is:

$$x_i(t) = Q_{ri}(t) / \left(\frac{\pi}{4} d^2\right) \quad (3\text{-}39)$$

When the volume of gas approaches the point of No. *i*+1 fracture, the time is $(t+(L_i-L_{i+1})/u_{gi})$ sec. The pressure is decreasing, the gas volume is enlarged and the flow rate increases. In the cross section of passage at this point, the occupied percentage of the gas phase increases. The occupied percentage of the liquid phase becomes smaller in the cross section of passage. Since the flow rate of the gas phase is greater than that of the liquid phase, the gas slippage phenomenon occurs. The gas volume is:

$$Q_{ri}(t + (L_i - L_{i+1})/u_{gi}) = \frac{P_{fi}(t) \cdot Q_{ri}(t)}{P_{fi+1}(t+(L_i-L_{i+1})/u_{gi})} \quad (3\text{-}40)$$

where $P_{fi}(t)$ is the pressure at the point of No. *i* fracture in the wellbore at time t, MPa; $P_{fi+1}(t)$ is the pressure at the point of No. *i*+1 fracture in the wellbore at time t, MPa; L_i is the distance from the point of No. *i* fracture to the wellbore bottom (Point II in Figure 3-13), m; L_{i+1} is the distance from the point of No. *i*+1 fracture to the wellbore bottom

(Point II in Figure 3-13), m; u_{gi} is the average flow rate of the gas and liquid mixture between the points of No. *i* and No. *i*+1 fractures, m/sec.

At the time ($(L_i-L_{i+1})/u_{gi}$), the gas volume from No. *i*+1 fracture is:

$$Q_{ri+1}(t+(L_i-L_{i+1})/u_{gi}) = 4\cdot(t+(L_i-L_{i+1})/u_{gi})\cdot L_{fi+1}\cdot H_{fi+1}(t+(L_i-L_{i+1})/u_{gi})$$

At this stage, the gas volume at the point of No. *i*+1 fracture in the wellbore is the sum of the two gas volumes above:

$$Q_{ri+(i+1)}(t+(L_i-L_{i+1})/u_{gi}) = Q_{ri}(t+(L_i-L_{i+1})/u_{gi}) + Q_{ri+1}(t+(L_i-L_{i+1})/u_{gi})$$

The true gas content $x_{i+1}(t)$ at the point of No. *i* fracture in the wellbore is:

$$x_{i+1}(t+(L_i-L_{i+1})/u_{gi}) = Q_{ri+(i+1)}(t+(L_i-L_{i+1})/u_{gi})/\left(\frac{\pi}{4}d^2\right) \quad (3\text{-}41)$$

i) Density of mixture of gas and liquid

Assuming 1 kg of gas, according to Boyle's law, we have:

$$P_s\cdot V_s = Z_s\cdot n\cdot R\cdot(T_s+273.15) \Rightarrow P_s\cdot\frac{1}{\rho_{gs}} = Z_s\cdot n\cdot R\cdot(T_s+273.15) \quad (3\text{-}42)$$

Equivalently, we get:

$$P\cdot\frac{1}{\rho_g} = Z\cdot n\cdot R\cdot(T+273.15) \quad (3\text{-}43)$$

$$\rho_g = \frac{P}{P_s}\cdot\frac{Z_s\cdot(T_s+273.15)}{Z\cdot(T+273.15)}\cdot\rho_{gs} \quad (3\text{-}44)$$

The density of the mixture of gas and liquid is:

$$\rho_m = \rho_g\cdot x_i + \rho_l\cdot(1-x_i) \quad (3\text{-}45)$$

where ρ_m , ρ_g and ρ_l is the density of the mixture of gas and liquid, the density of gas and the density of liquid at P and T, respectively, kg/m^3; ρ_{gs} is the gas density under the standard conditions, 0.717 kg/m^3; P is the pressure at time t, MPa; T is the temperature at time t, °C; Ps is the pressure under standard conditions, 0.10 MPa; Ts is the standard

temperature, 15°C; Zs is the gas compressibility coefficient under the standard conditions, dimensionless; Z is the gas compressibility coefficient under the conditions of P and T, dimensionless; R is the ideal gas constant, 8.314 J/(K.mol); n is the mole of gas, mol.

ii) Average flow rate of gas and liquid mixture

$$u_m = \frac{\rho_g \cdot Q_{gi} + \rho_l \cdot Q_l}{A \cdot \rho_m} = \frac{\rho_g \cdot Q_{gi} + \rho_l \cdot (\frac{\pi}{4} d^2 - Q_{gi}) \cdot u_B}{\frac{\pi}{4} d^2 (\rho_g \cdot x_i + \rho_l \cdot (1 - x_i))} = \frac{\rho_g \cdot Q_{gi} / \frac{\pi}{4} d^2 + \rho_l \cdot u_B (1 - Q_{gi} / \frac{\pi}{4} d^2)}{\rho_g \cdot x_i + \rho_l \cdot (1 - x_i)} \quad (3\text{-}46)$$

where Qgi is the gas volume at the point of No. *i* fracture at time t, m^3/sec; Q_l is the liquid volume at time t, m^3/sec.

iii) Pressure drop along the horizontal path

$$P_{fi}(t) - P_{fi+1}(t) = \lambda(t) \cdot \frac{1}{d} \cdot \frac{u_m^2(t)}{2} \cdot \rho_m(t), \ (i = 1, 2, \dots, n-1) \quad (3\text{-}47)$$

where $P_{fi}(t)$is the pressure at the point of No. *i* fracture in the wellbore at time t, MPa; $\lambda(t)$is the friction resistance coefficient along the wellbore at time t; $u_m(t)$ is the average flow rate of the mixture of gas and liquid at time t, m/sec.

3) Flowing along the slanted path during two-phase flow

This is a nonisothermal process along the slanted section (section II – III in Figure 3-13). An empirical temperature gradient is set up. Chen J. (1983) and Baker O. (1957) proposed that the pressure drop along the slanted section of wellbore during two-phase flow is calculated with this formula:

$$P_{III}(t) - P_{wf}(t) = Fe(t) \cdot \rho_m(t) \cdot g \cdot LS \cdot sin\theta + \lambda(t) \cdot \frac{1}{d} \cdot \frac{u_m^2(t)}{2} \cdot \rho_m(t) \quad (3\text{-}48)$$

4) Flowing along the vertical path during two-phase flow

Chen J. (1979) derived a model to calculate the pressure drop along the vertical path of wellbore during two-phase flow, considering the gas slippage effect. It is assumed that it does not work to the environment outside when the mixture of gas and liquid is flowing through the vertical wellbore (section III – IV shown in Figure 3-13) from bottom to top. It is a nonisothermal process and an empirical temperature gradient is set up in the calculation. The pressure drop along the vertical section is described as:

$$P_{III}(t) - P_{wh}(t) = \rho_m(t) \cdot g \cdot \Delta h \cdot (1 + \frac{\lambda(t) \cdot u_m^2(t)}{2 \cdot g \cdot d}) \quad (3\text{-}49)$$

5) Flowing through the choke during two-phase flow

Ashford F. E. (1974) stated that it is a multi-variation process when the mixture of gas and liquid goes through a choke. A tiny section of a choke is selected (dL >0) and the gas and liquid distribute evenly in the selected volume. Since it is a multi-variation process, for a unit mass of fluid, we have:

$$P \cdot V_g^n = b \quad (3\text{-}50)$$

where P is the pressure in the system at time t, MPa; Vg is the gas volume in a unit mass of gas, m^3; n and b are the multi-variation constants when the mixture of gas and liquid is flowing through the choke, dimensionless.

From Bernoulli's equation, we have:

$$\frac{P_{wh}(t)}{\rho_m(t)} + \frac{u_m^2(t)}{2} = \frac{P_0}{\rho_m(t)} + \frac{v_{mc}^2(t)}{2} + \xi \cdot \frac{v_{mc}^2(t)}{2} \quad (3\text{-}51)$$

where P_0 is the setup pressure at the outlet of the choke, MPa; v_{mc} is the flow velocity of the mixture of gas and liquid at the outlet of the choke at time t, m/sec; ξ is the local resistance coefficient when the fluid is flowing through the choke, dimensionless.

Note that:

$$\frac{n}{n-1}\cdot V_g\cdot P_{wh}(t)\cdot\left[\left(\frac{P_0}{P_{wh}(t)}\right)^{\frac{n-1}{n}}-1\right]+V_l\cdot\left(P_0-P_{wh}(t)\right)$$

$$=\frac{1}{2}\left(v_{mc}^2(t)+\xi\cdot v_{mc}^2(t)-u_m^2(t)\right) \quad (3\text{-}52)$$

where V_l is the liquid volume in a unit mass of liquid, m^3;

From continuity equation: $u_m\cdot\frac{\pi\cdot d^2}{4}=v_{mc}\cdot\frac{\pi\cdot d_c^2}{4}$, where d_c is the choke diameter, m.

Solving the abovementioned equations together, the relationship curve of $P_{wh}(t)$ vs. d_c is determined. This means that the choke size can be adjusted dynamically with wellhead pressure alteration over time.

Chapter 4 SIMULATOR DEVELOPMENT

4.1 Flow process diagram of the simulator

Based on the theoretical model in Chapter 3, the flow process diagram of the simulator is built, as shown in Figure 4-1.

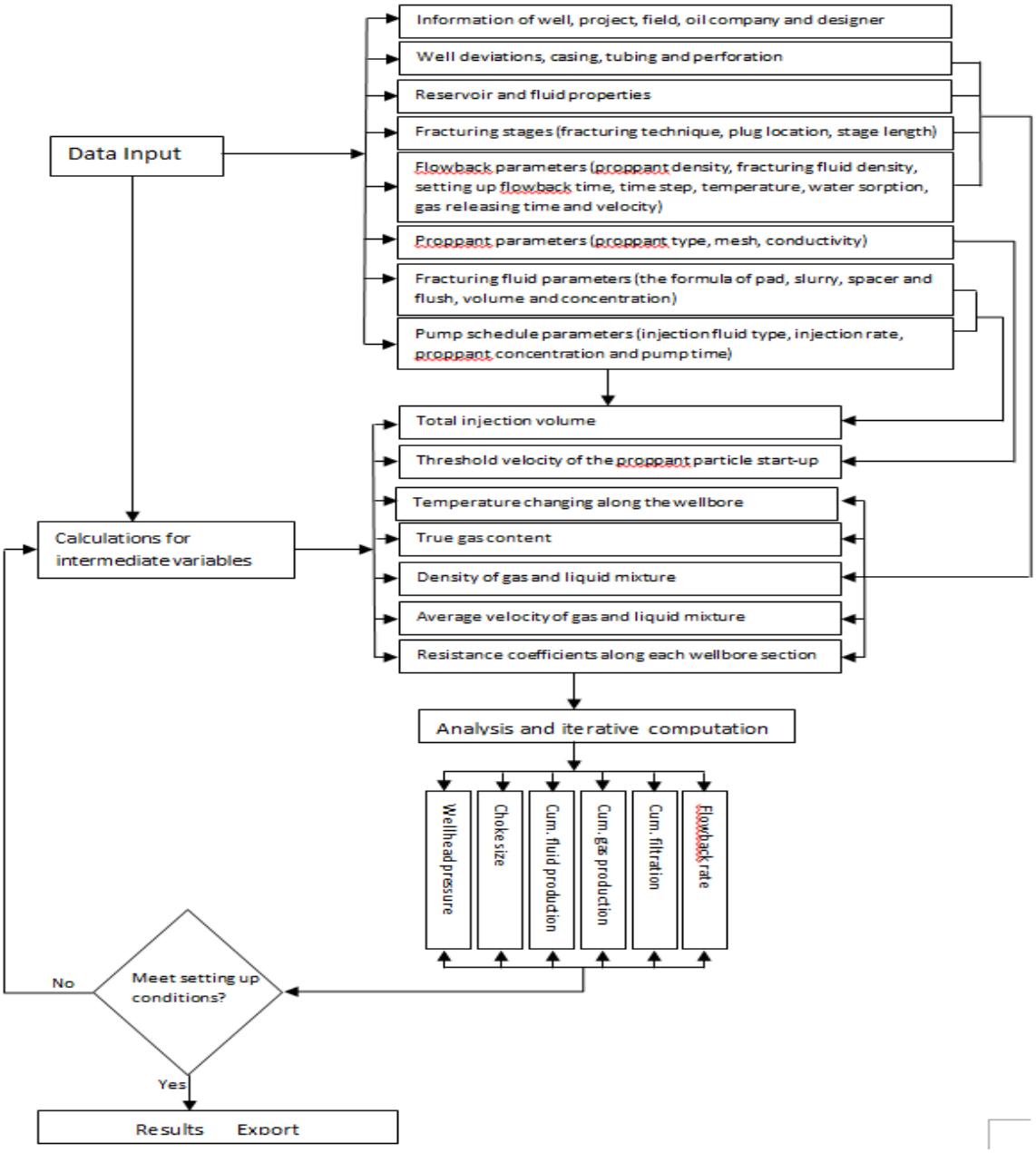

Figure 4-1 Flow process diagram of the simulator

4.2 Principles for simulator development

1) Integrity development and modular structure

A great amount of information is involved in the simulator and the required data is diverse. The exported results are different from each other. When the simulator is developed, it is considered as an integrity and divided into many independent modules at the same time. The fundamental calculations are placed in the modules, which avoids the complex changing-over process of computing windows.

2) Independence of modules

According to the theory of software engineering, a simulator is divided into many independent modules. It is not only convenient for development but also for users to operate the simulator more easily. The more important thing is that the simulator is prone to maintenance and improvement. The simulator is parted as modules based on their functions. Each module is independent. Meanwhile, it is correlated with others through data flow.

3) Easy operation

The simulator provides the menu-type operations. Meanwhile, the pop up and pull down menus are supported. The common Windows interface is utilized, which is friendly and easy to operate.

4.3 Development and operation settings

Development settings: Windows 7 (professional).

Coding language: C++ language.

Development toolkits: C++ language, QT, Microsoft Word 2010, and Microsoft Excel 2010.

Operation settings: Windows 7 and plus.

Hardware: CORE i3 and plus.

4.4 Introduction of the simulator structure and functions

This work focuses on the development of a simulator, coded with C++ language and realizing its interface with QT. The simulator provides the necessary information to successfully achieve production and economic goals of hydraulic fracturing in shale gas reservoirs. It contains five fully integrated modules used for a fracking stage design, a proppant design, a fracturing fluid design, flowback optimization, production analysis and forecasting, and economic optimization, as shown in Figure 4-2. It includes utilities for proppants, a fracking fluid formula and the implementation for typical shales, importing and exporting data and generating output reports. The simulator is able to input all types of data, including rock properties, fracturing stages, fracturing fluids, proppants, well configuration and economics. The flowback section is completed and the simulator is capable of performing dynamic adjustment of a choke size while wellhead pressure changes over time with a two-phase (gas and liquid) flow model along the horizontal, slanted and vertical sections. This model simultaneously considers forces acting on proppant particles, filtration loss of water, compressibility of a fracturing fluid, wellbore friction, a gas slippage effect, water absorption and adsorption.

The fundamental procedure for the simulator development is to improve the interface and functions of the simulator. This required a review of the literature and consultation with industrial and academic professionals. The mathematical model was built to optimize the choke size as wellhead pressure changed over time with a two-

phase (gas and liquid) flow model along the horizontal, slanted and vertical sections. Next, the interface is realized with QT and the computer codes with C++ language were written to run the interface.

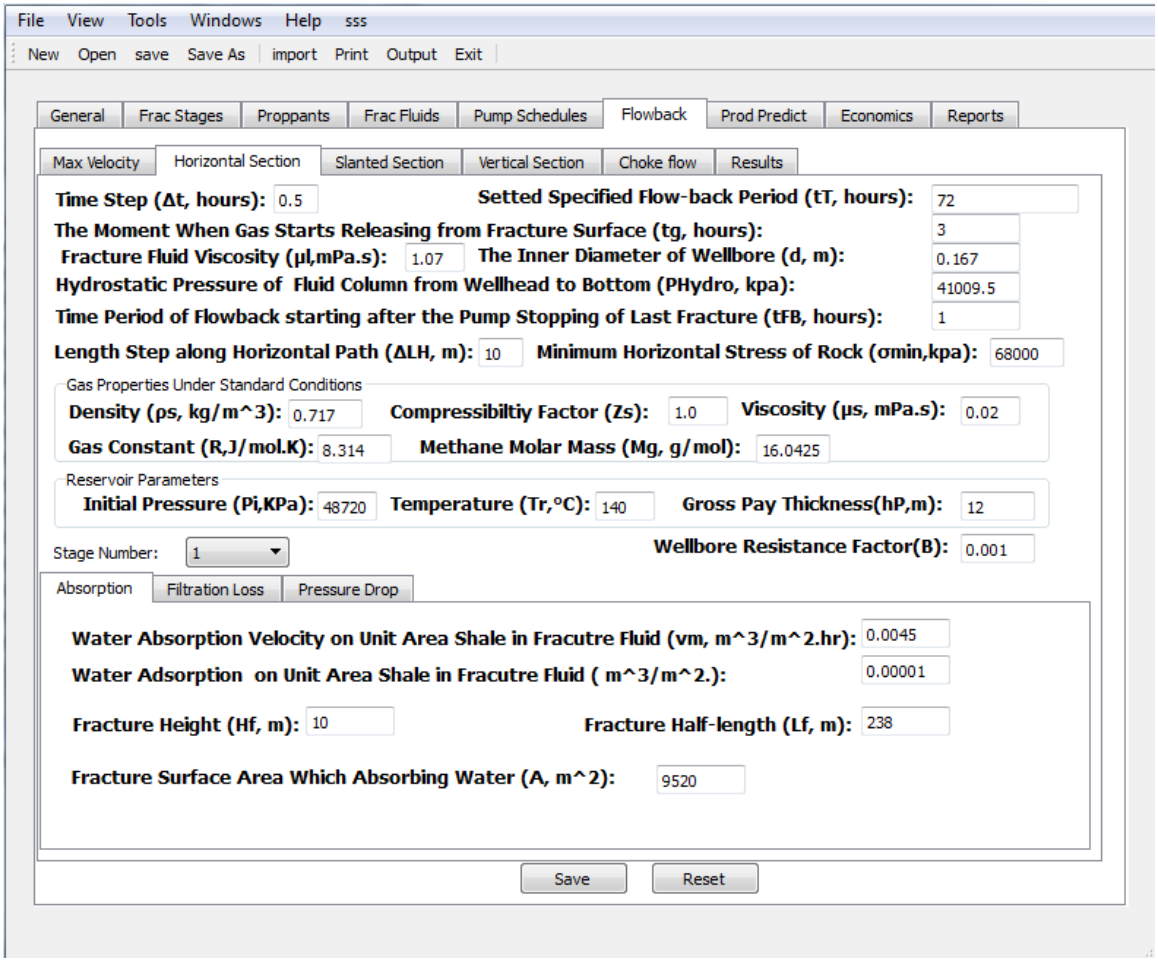

Figure 4-2 Simulator interface picture including the main modules

4.5 Simulator development through coding with C++ language

Stroustrup B. (1979) stated that C++ language is a general-purpose programming language. It has imperative, object-oriented and generic programming features. It provides facilities for low-level memory manipulation. It was published with the International Organization for Standardization (ISO) in December 2014. It is

characterized with efficiency and flexibility, providing high-level features for program organization. The coding files are illustrated as follows.

1) Global variables file

The global variables are defined in this file, such as a shale name, monetary, unit price and fluid amount unit.

2) General variables file

In the file, general parameters are defined: information on the oil company, design company, designer, field, well and project. General wellbore parameters are also defined in the tab of wellbore, including casing, tubing, deviation and perforation. General reservoir properties parameters are defined in the properties tab.

3) Fracturing stages parameters file

Fracturing stages variables are defined in this file: a fracturing technique, a plug location and stage length are found here.

4) Proppant parameters file

In the file, proppant parameters are defined: a proppant particle size, conductivity, a proppant type and shape.

5) Fracturing fluid parameters file

This file is divided into four sections: pad, slurry, spacer and flush. The related parameters are defined: unit price, concentration, amount and cost. The formula of pad, slurry, spacer and flush can be displayed in the file.

6) Pump schedule parameters file

In this file, the pump schedule parameters are defined, for example, the injection fluid type, proppant type, proppant concentration at the bottom hole, injected proppant amount, cumulative injected proppant amount and pump time.

7) Flowback parameters file

This file is made up of six parts: max velocity, horizontal section, slanted section, vertical section, choke flow and results. The related parameters are defined in setting up flowback time, the density of a fracturing fluid, the proppant density, the length of each wellbore section and temperature.

8) Codes application programs

The codes application programs are written in corresponding *.cpp files, respectively. They contain the programs that carry out the functions: initial values assignment, data importing and exporting. In the application file of ShaleGasMainWindow.cpp, many functions are involved. The corresponding variables from the interface to the files, data calculations and output are also included.

Chapter 5 VALIDATION OF DEVELOPED SIMULATOR WITH REAL SHALE GAS RESERVOIR DATA FROM FIELD OPERATIONS IN CHINA

5.1 Introduction

In this chapter, the new simulator testing procedure is applied to a shale gas well from the Shuangyang Formation in China. The thickness of the targeted formation is estimated to be 12 m, its porosity is 6.95% and its permeability is 0.0018 mD. This well is horizontally drilled and completed with cement and casing. The True Vertical Depth is 4,060 m and the length of the horizontal section is 600 m, as shown in Figure 5-1. From a core sample analysis, the materials are mainly quartz (68.2%) and clay (14.3%). The brittleness coefficient is calculated at 68.5%, which is preferential to being brittle. In terms of well testing data, Young's Modulus is 3.078×10^4 MPa, Poisson's Ratio is 0.24, the rock stress of the overburden interlayer is 73 MPa and the minimum horizontal stress is 68 MPa, as shown in Figure 5-2. It is an appraisal well and hydraulically fractured in three stages. On average, the stages are spaced 200 m apart and the half-length of fractures is 238m. It is stimulated completely with 5,965.5 m^3 of fracturing fluid (water, proppant and chemicals). The simulation data in the simulator testing is found in Table 5-1.

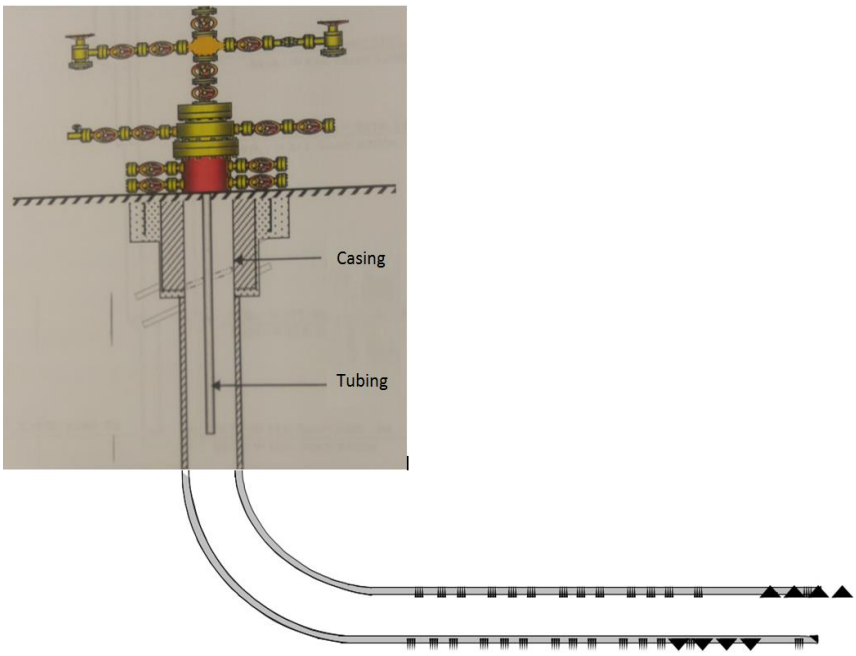

Figure 5-1 Scheme picture of well configuration

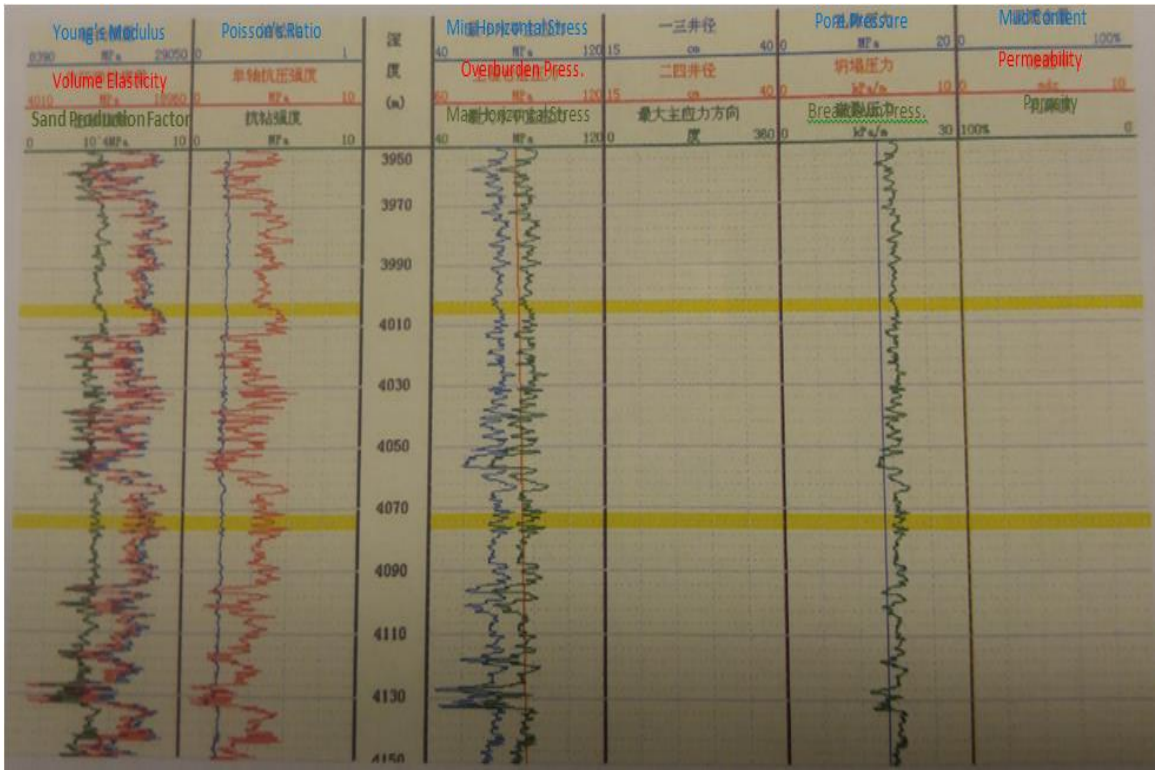

Figure 5-2 Formation properties from well testing dada analysis

Table 5-1 Simulation data from field operations

Name	Value		Name	Value
Date	01/09/2017		Time step	0.5 hours
Formation thickness	12 m		Length step	10 m
Porosity	6.95%		Setting up flowback time	72 hours
Permeability	0.0018 mD		The time that gas starts releasing	3 hours
True Vertical Depth	4,060 m		Fracturing fluid density	1030 kg/m^3
The length of horizontal section	600 m		Fracturing fluid viscosity	1.07 mPa.s
Young's modulus	30780 MPa		Proppant density	2600 kg/m^3
Poisson's Ratio	0.24		Wellbore diameter	0.167
The minimum horizontal stress	68 MPa		Rock compressibility	5.0E-06 1/kpa
Initial Pressure	48.72 MPa		Breakdown pressure	77 MPa
Formation Temperature	140 °C		Total injection volume	5,965.5 m^3

5.2 Results and discussion

When the required data for the simulator are successfully input, the analytical model automatically and quickly performs the calculation. By selecting results tab in Flowback, the simulation outcomes are shown in the form, as shown in Figure 5-3. The wellhead pressure, choke size, cumulative fluid production, cumulative gas production, cumulative filtration and flowback rate are expressed following each time step in the simulation over time. According to the exported data, the comparison and analysis curves are drawn in Figures 5-4 to 5-8.

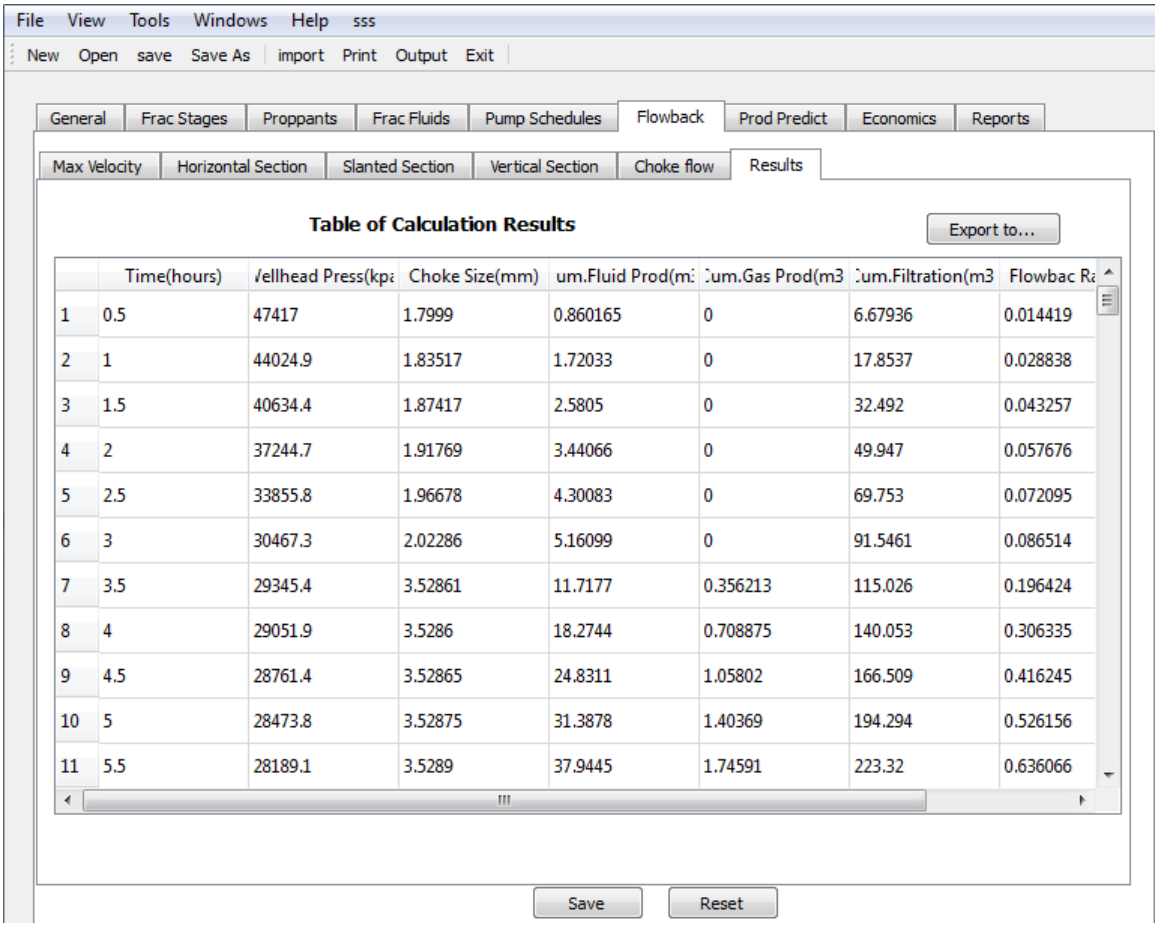

	Time(hours)	/ellhead Press(kpa	Choke Size(mm)	um.Fluid Prod(m:	:um.Gas Prod(m3	:um.Filtration(m3	Flowbac Ra
1	0.5	47417	1.7999	0.860165	0	6.67936	0.014419
2	1	44024.9	1.83517	1.72033	0	17.8537	0.028838
3	1.5	40634.4	1.87417	2.5805	0	32.492	0.043257
4	2	37244.7	1.91769	3.44066	0	49.947	0.057676
5	2.5	33855.8	1.96678	4.30083	0	69.753	0.072095
6	3	30467.3	2.02286	5.16099	0	91.5461	0.086514
7	3.5	29345.4	3.52861	11.7177	0.356213	115.026	0.196424
8	4	29051.9	3.5286	18.2744	0.708875	140.053	0.306335
9	4.5	28761.4	3.52865	24.8311	1.05802	166.509	0.416245
10	5	28473.8	3.52875	31.3878	1.40369	194.294	0.526156
11	5.5	28189.1	3.5289	37.9445	1.74591	223.32	0.636066

Figure 5-3 Simulation data form

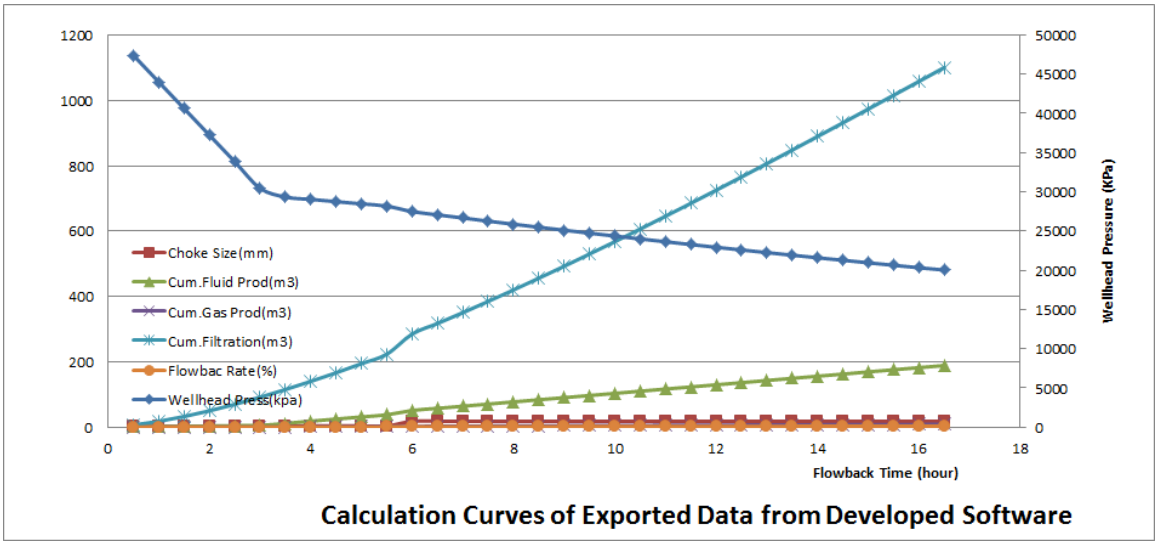

Figure 5-4 Calculation curves of exported data from developed simulator

In Figure 5-4, the exported data from simulation creates the curves following each time step in the simulation. It reveals that the wellhead pressure, choke size, cumulative fluid production, cumulative gas production, cumulative filtration and flowback rate are altering over time.

For the curve of cumulative filtration, in 16.5 hours after the flowback operation began, the pressure in fractures is greater than the formation pressure, and thus, the fracturing fluid permeates into the formation continuously across the fracture faces. Most of the fracturing fluid is retained in the hydraulically induced fractures, and reactivated natural microfractures and micropores in the invaded zone. The exact number of secondary and natural fractures cannot be identified because the data of the fracture shape and geometry in the well is deficient. From the curve, about 21% of the injected volume is held in the region. In addition, the curve indicates that the cumulative filtration increases over time. After the gas starts releasing, it turns into two-phase flow. Correspondingly, the fracturing fluid leaks faster. This may be caused by the water substituting the spots of gas in the invaded zone.

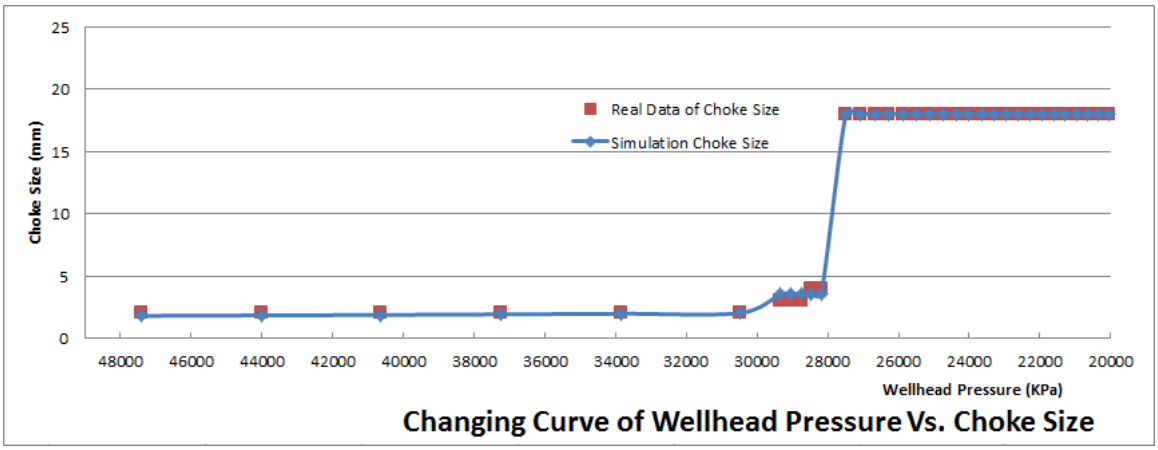

Figure 5-5 Changing curve of wellhead pressure vs. choke size

In Figure 5-5, the changing curves of wellhead pressure vs. the choke size of real data and simulation data are illustrated. It was determined that as wellhead pressure drops, the choke size becomes larger. Real and simulation data match each other very well. The curve looks like an inversed “S”. At the beginning, during the pure liquid flow, the wellhead pressure drops very fast; however, the choke size almost does not change in the wellhead and it keeps unchanged in the real data. After the gas starts releasing, it turns into two-phase flow. The wellhead pressure has a slow drawdown and the choke size enlarges a little. As the wellhead pressure continues to drop until the pressure in fractures is less than the minimum horizontal stress of the rock, the hydraulic fractures are closed and the proppant particles are clamped tightly in the fractures. The maximum choke size is changed to use and the wellhead pressure furthers to drop.

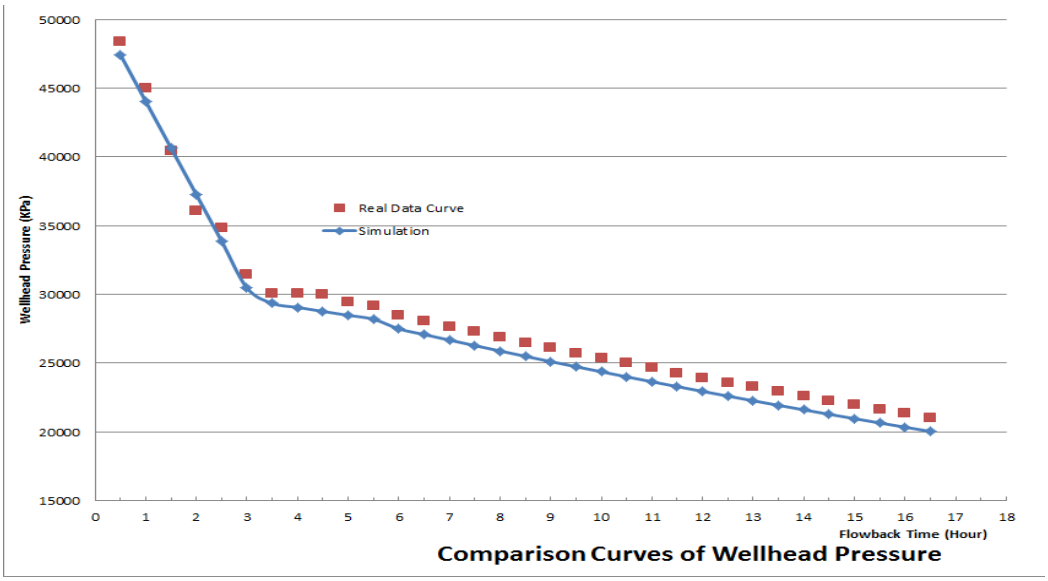

Figure 5-6 Comparison curves of wellhead pressure

Figure 5-6 presents the comparison curves of wellhead pressure. On the whole, it shows a good fit. Both real and simulation data have the identical changing

tendencies. Note that the simulation results presented herein are slightly different from the real data. It could be caused by the heterogeneous properties, adjacent operational work or well interference that is not considered in the analytical model utilized herein. Frequently, misfits could be encountered during the studies. A different filtering method should be used to approach another solution. Alternatively, a compromising result could be chosen in favor of the objectives. For the presented example, the wellhead pressure is probably an artifact of reporting and not a feature of the well. In this case, it is reasonable to compromise the history match of the wellhead pressure in favor of improving the match of a choke size, cumulative fluid production, cumulative gas production and a flowback rate. Finally, the case does not have a unique result, and thus, multiple solutions are acceptable. This phenomenon is also obvious in the data of cumulative fluid production, cumulative gas production and a flowback rate, but is less remarkable, as shown in Figures 5-7 and 5-8.

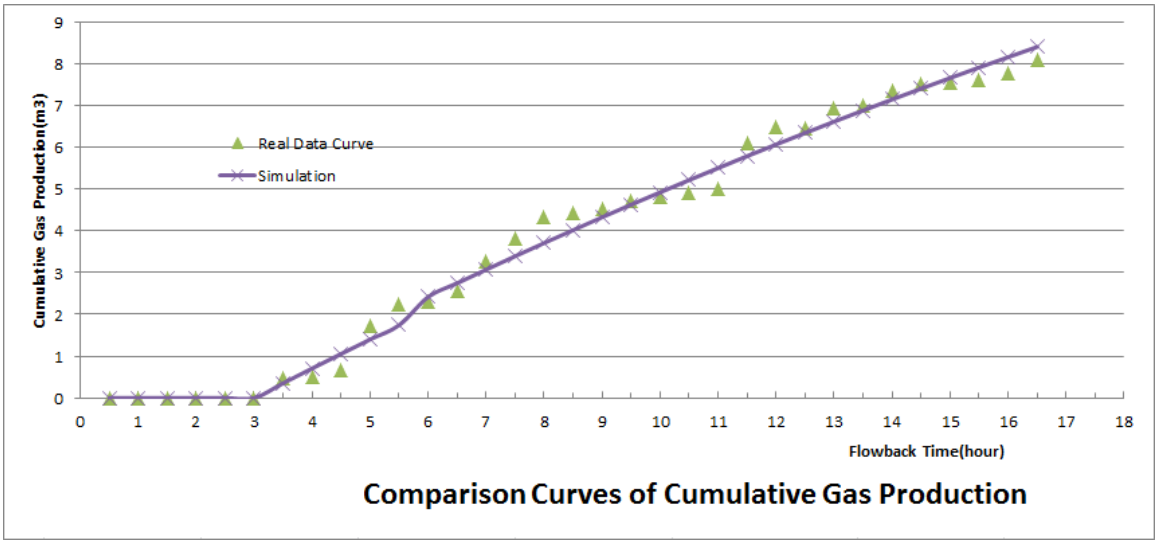

Figure 5-7 Comparison curves of cumulative gas production

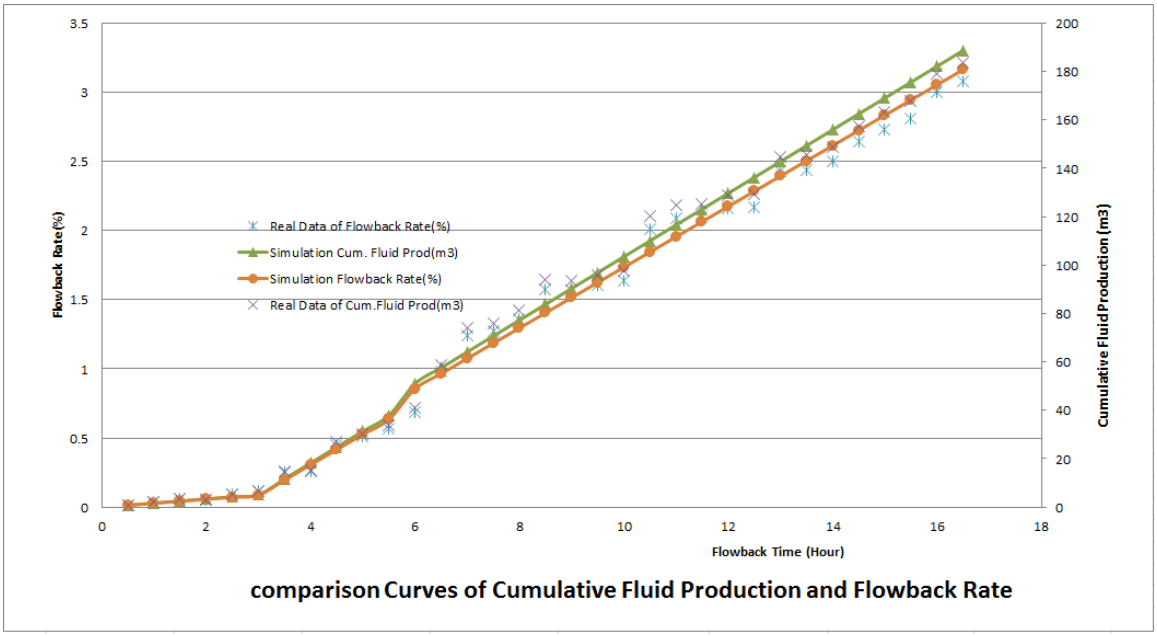

Figure 5-8 Comparison curves of cumulative fluid production and flowback rate

Both real and simulation data have the identical changing tendencies and match each other very well. The simulation curves are obviously smooth, while the real data curves change sharply at some points. The novel procedure contains flowback data during the matching process to improve the conversion results. It also deals with the misfits of each of the wellhead pressure, cumulative fluid production, cumulative gas production and flowback rate as independent objectives and minimizes the discrepancies using multi-objective optimization. This method is especially beneficial when the flowback data is noisy. In this work, the essential groundwork for future research during flowback as well as production is provided, which demands a more accurate reservoir and fluid model with viable rock and fracture characteristics.

Chapter 6 CONCLUSIONS AND RECOMMENDATIONS

6.1 Conclusions

The major contributions and conclusions of this work are:

1. A mathematical model for optimizing a choke size as wellhead pressure changes over time is built. This optimization model is capable of performing dynamic adjustment of a choke size while wellhead pressure changes over time with a two-phase (gas and liquid) flow model as fractures are closing along horizontal, slanted and vertical sections. The forces acting on proppant particles, filtration loss of water, compressibility of a fracturing fluid, wellbore friction, a gas slippage effect, water absorption and adsorption are simultaneously considered in this model.
2. When the pressure in fractures is greater than the formation pressure, the theoretical feasibility of gas releasing from shale faces is identified due to the capillary pressure and substitution. Using an idealized straight smooth capillary model, it is concluded that the join forces of capillary pressure and formation pressure are greater than the pressure in fractures in the non-water-wetting sections. This allows the gas to move and be produced.
3. The maximum flowing velocity of a liquid is identified considering the forces acting on proppant particles.
4. The equations for a pressure drop in two-phase (gas + liquid) flow are derived while considering a slippage effect and friction loss along horizontal, slanted and vertical paths.

5. Through reading papers and consulting professionals, the workflow of hydraulic fracturing and fracture cleanup were investigated, and a design was developed for the interface and functions of a novel simulator. It includes utilities for proppants, a fracturing fluid formula and implementation for typical shale, importing and exporting data and generating output reports.
6. The new simulator is successfully written using code with C++ language and realizing the interface with QT. The interface is realized with QT and the computer codes with C++ language are written to run the interface. Currently, the flowback section is completed and the simulator is capable of performing dynamic adjustment of a choke size while wellhead pressure changes over time with a two-phase (gas and liquid) flow model as fractures close along the horizontal, slanted and vertical sections simultaneously.
7. A novel simulator testing procedure is applied to a shale gas well from the Shuangyang Formation in China. In the exported data, the wellhead pressure, choke size, cumulative fluid production, cumulative gas production, cumulative filtration and flowback rate are demonstrated following each time step in the simulation over time. Comparison curves with both real and simulation data are demonstrated, respectively.
8. Both real and simulation data has the identical changing tendencies and match each other very well. The simulation curves are obviously smooth, while the real data curves change sharply at some points.

6.2 Recommendations for future work

The following recommendations are for future work:

1. Only the period when the pressure in fractures is greater than the formation pressure is studied. After the pressure in fractures turns smaller than the formation pressure, the gas production starts and the complex percolation with two phases in the reservoir governs flow considering the relative permeability of gas and water.
2. A large amount of real data from field development is needed to generalize the relationship between flow-back rates of a total injected volume vs. future production.
3. The equations for future production performance forecasting considering heterogeneous fracture properties need to be derived.
4. The economic models considering CAPEX, OPEX, revenue, royalty and tax needs to be built to optimize the field operations.

References

Adefidipe, O.A., Xu, Y. 2014. Immediate Gas Production from Shale Gas Wells: A Two-Phase Flowback Model. Presented at the SPE Unconventional Resources Conference, Woodlands, 1-3 April. SPE-168982-MS.

Alkouh, A. B., and Wattenbarger, R. A. 2013. New Advances in Shale Reservoir Analysis Using Flowback Data. Paper SPE 165721 presented at 2013 SPE Eastern Regional Meeting, Pittsburgh, Pennsylvania, USA, 20 - 22, August. http://dx.doi.org/10.2118/165721-MS.

Ashford. F.E. 1974. An Evaluation of Critical Multi-phase Flow Performance through Wellhead Chokes, J.P.T., 8.

Ayoub, J.A., Hutchins, R.D., van der Bas, F. 2006. New Findings in Fracture Clean-up Change Common Industry perceptions. Society of Petroleum Engineers. Doi:10.2118/98746-MS.

Baker, O. 1957. Effect of Hills on Two-phase Pressure Drop. Oil and Gas J., 11.

Bertuzzi, A.F., Tek, M.R. and Poettmann F.H. 1956. Simultaneous Flow of Liquid and Gas Through Horizontal Pipe. Trans., AIME. 17-24.

Binazadeh M, Xu M, Zolfaghari A. 2015. Effect of Electrostatic Interactions on Water Uptake of Gas Shales: The Interplay of Solution Ionic Strength and Electrostatic Double Layer[J]. Energy & Fuels.

Blasingame, T.A. 2008. The Characteristic Flow Behavior of Low-Permeability Reservoir Systems. Paper presented at the SPE Unconventional Reservoirs Conference, 103 Keystone, Colorado, USA. Society of Petroleum Engineers SPE-114168-MS. DOI: 10.2118/114168-ms.

Blaskovich, F.T., Gain, G.M. and Sonier, F. 1993. A Multicomponent Iso-thermal System for Efficient Reservoir Simulation. Presented at the Middle East Oil Technical Conference of the Society of Petroleum Engineers, Manama, 14-17 March. SPE-11480-MS.

Boyer, C., Kieschnick, J., Suarez-Rivera, R., Lewis, R. E., Waters, G., 2006. Producing gas from its source. Oilfield Review, 18, 36-49.

B. V. Derjaguin, N. V. Churaev, V. M. Muller. 1987. Surface Forces. Consult. Bur., New York.

Cavalcante Filho, J.S.m, Shakiba, M. 2015. Implementation of a Preprocessor for Embedded Discrete Fracture Modeling in an IMPEC Compositional Reservoir Simulator. Presented at the SPE Reservoir Simulation Symposium, Houston, 23-25 February. SPE-173289-MS.

Chekani, M., Bagherpour, M.H., Alavi, M.F. 2010. Novel Approach to Mitigate Gas Production in a High Gor Carbonate Reservoir with Drilled Wells—Case Study. Paper presented at the SPE Production and Operations Conference and Exhibition, Tunis, Tunisia. Society of Petroleum Engineers SPE-135875-MS. DOI: 10.2118/135875-ms.

Chen, J. 1989. Two-phase Fluid Flow of Petroleum Gas and Liquid in Pipes. [M]: Petroleum Industry Press.

Chen, J. 1979. Pressure Drop Calculation in Vertical Wellbores with the Mixture of Oil, Gas and Water. [J]: Petroleum Exploration and Development. No. 2.

Chen, J. 1983. Comprehensive Description of Pressure Drop Calculation Methodologies of Multi-phase Fluid flow with Gas and Liquid in Direction Wells. [J]: Journal of Daqing Petroleum Institute, No. 4.

Chen Z., Zhang S., Shen M. 1996. Potential Hazards of Clay Minerals in Oilfield Protection [J]. Journal of Chengdu Institute of Technology, 23(2): 80-87.

Choi, S. and Seungjoo, K. 2001. Theoretical and Probabilistic Analyses of Incipient Motion of Sediment Particles. KSCE Journal of Civil Engineering 5.1: 59-65.

Churaev, N. V., 1995 (a). Contact angles and surface forces. Advances in Colloid & Interface Science, 58(58), 87-118.

Churaev, N. V., 1995 (b). The relation between colloid stability and wetting. Journal of Colloid & Interface Science, 172(2), 479-484.

Churaev, N. V., Starke, G., Adolphs, J. 2000. Isotherms of capillary condensation influenced by formation of adsorption films: 1. calculation for model cylindrical and slit pores. Journal of Colloid & Interface Science. 221(2), 246–253.

Crafton, J.W. and Gunderson, D.W. 2007. Stimulation Flowback Management: Keeping a Good Completion Good. Presented at the SPE Annual Technical Conference and Exhibition, Anaheim, 11-14 November. SPE-110851-MS.

Cipolla, C.L., Warpinski, N.R. 2008. The Relationship Between Fracture Complexity, Reservoir Properties, and Fracture Treatment Design. Presented at the SPE Annual Technical Conference and Exhibition, Denver, 21-24 September. SPE-115769-MS.

Cinco-Ley, H. and Samaniego-V., F. 1981. Transient Pressure Analysis: Finite Conductivity Fracture Versus Damaged Fracture Case Paper SPE 10179 presented at the SPE Annual Technical Conference and Exhibition, San Antonio, Texas, USA. 4-7 October. Doi:10.2118/10179-MS.

Cipolla, C.L., Lolon, E. 2009. Modeling Well Performance in Shale-Gas Reservoirs. Paper SPE 125532 presented at the SPE/EAGE Reservoir Characterization and Simulation Conference, Abu Dhabi, UAE, 19-21 October. Doi:10.2118/125532-MS.

Clarkson, C.R., and Willams-Kovacs, J. 2013a. Modeling Two-Phase Flowback of Multifractured Horizontal Wells Completed in Shale. SPE Journal. 18(04): 795-812. SPE-166214-MS.

Clarkson, C.R., and Willams-Kovacs, J. 2013b. A New Method for Modeling Multi-Phase Flowback of Multi-Fractures Horizontal Tight Oil Wells to Determine Hydraulic Fracture Properties. Presented at the SPE Annual Technical Conference and Exhibition, New Orleans, 30 September-02 October. SPE-16621-MS.

Colebrook, C.F. 1933. Turbulent Flow in Pipes with Particular Reference to the Transition Region Between the Smooth and Rough Pipe Laws. J. Inst. Civil. 133.

Cooke, C.E. Jr. 1975. Effect of Fracturing Fluids on Fracture Conductivity. J Pet Technol 27(10): 1273-1282; Trans., AIME, 259. SPE-5114-PA. doi: 10.2118/5114-PA.

Curtis J B. 2002.Fractrured shale-gas systems[J]. AAPG Bulletin, 86(11); 1921-1938.

Dean, R.H. and Lo, L. 1988. Simulations of Naturally Fractured Reservoirs. SPE Reservoir Engineering. 3(02): 638-648. SPE-1410-PA.

Dehghanpour, H., Zubair, H. A., Chhabra, A., & Ullah, A. 2012. Liquid intake of organic shales. Energy Fuels, 26(9), 5750-5758.

Dehghanpour H, Lan Q, Saeed Y. 2013. Spontaneous imbibition of brine and oil in gas shales: effect of water adsorption and resulting microfractures[J]. Energy & Fuels, 27(6): 3039-3049.

Dutta, R., Lee, C. H., Odumabo, S., Ye, P., Walker, S.C., Karpyn, Z.T., and Ayala, L.F. 2012. Quantification of Fracturing Fluid Migration due to Spontaneous Imbibition in Fractured Tight Formations. Paper SPE 154939 presented at SPE Americas Unconventional Resources Conference, Pittsburgh, Pennsylvania USA, 5-7 June. http://dx.doi.org/10.2118/154939-MS.

Exxon Annual Report 2006［R］. Exxon，2006.

Ezulike, D.O., Dehghanpour, H., and Hawkes, R.V. 2013. Understanding Flowback as a Transient Two-Phase Desplacement Process: An Extension of the Linear Dual-Porosity Model. Presented at the CPR Unconventional Resources Conference-Canada, Calgary, 5-7 November. SPE-167164-MS.

Ezulike, D.O., Dehghanpour, H., and Virues, C.J. 2014. A Flowback-Guided Approach for Production Data Analysis on Tight Reservoirs. Presented at the 2014 SPE/CSUR

Unconventional Resources Conference-Canada, Calgary, 30 September-2 October. SPE-171636-MS.

Flanigan O. 1958. Effect of Uphill Flow on Pressure Drop in Design of Two-phase Gathering Systems. Oil and Gas J., 10.

Friedel, T. 2006. Numerical Investigation on Hydraulic Fracture Cleanup and Its Impact on the Productivity of a Gas Well with a Non-Newtonian Fluid Model. Paper SPE 99445 presented at the SPE Gas Technology Symposium, Calgary, 15-17 May. Doi: 10.2118/99445-MS.

Fredd, C.N., McConnell, S.B. 2001. Experimental Study of Fracture Conductivity for Water-Fracturing and Conventional Fracturing Applications. SPE J. 6(3): 288-298. SPE-74138-PA. doi: 10.2118/74138-PA.

Fossa, A., Ostebo, B. 2007. Harsh Environment HPHP Gas-Condensate Production Clean-up Experiences – Kristin Field. Society of Petroleum Engineers. Doi:10.2118/108656-MS.

Fu X., Qin J. 2011. Mineral Composition Characteristics of Hydrocarbon Source Rocks and Geological Significance of Gas Confiscation: a Case Study of High Quality Source Rocks of Paleozoic Marine Rocks in the Upper Middle Yangtze River [J], Petroleum Exploration and Development, 38(6): 671-684.

Gandossi, L. and Von Estorff, U. 2015. An Overview of Hydraulic Fracturing and Other Formation Stimulation Technologies for Shale Gas Production. EUR 26347; doi:10.2790/379646.

Gao, S., Bian, C. and He, S. 2004. Starting Pressure of Low Permeability Cores by Using Mercury Injection Method. [J]: Petroleum Exploration and Development. 2004(6), Vol31(3): 140-142.

Gao, S., Hu, Z., Guo, W. 2013. Water Absorption Characteristics of Gas Shale and the Fracturing Fluid Flowback Capacity. [J]: Natural Gas Industry. 2013(12), Vol33(12): 1-6.

Gdanski, R.D. Fulton, D.D., and Shen, C. 2009. Fracture-Face-Skin Evolution During Cleanup. SPE Prod & Oper 24 (1): 22-34. SPE-101083-PA. doi:10.2118/101083-PA.

Gdanski R. and Weaver J. 2005. Fracture Face Damage- It Matters. Paper SPE 94649 presented at the SPE European Formation Damage Conference, Scheveningen, The Netherlands, 25-27 May. Doi: 10.2118/94649-MS.

Gensterblum Y., Ghanizadeh A. and Krooss B.M. 2014a. Fluid-dynamical and poroelastic coupling of gas permeability of inert and sorbing gases on an Australian sub-bituminous coal. J. Nat. Gas Sci. Eng.

Gensterblum Y., Ghanizadeh A. and Krooss B.M., 2014b. Gas permeability measurements on Australian subbituminous coals: fluid dynamic and poroelastic aspects. J. Nat. Gas Sci. Eng. 19, 202–214.

Green D.P., Dick J.L. and McAloon M. et al. 2008. Oil-water imbibition and drainage capillary pressure determined by MRI on a Wide Sampling of Rocks. Paper prepared for presentation at the International Symposium of the Society of Core Analysts held in Abu Dhabi, UAE 29 October-2 November, 2008.

Glover P. 2010. Formation Evaluation-Petroleum Geology. [M] Department of Geology and Petroleum Geology, University of Aberdeen, the United Kingdom.

Haidar S. and Rylance M. 1996, January. Novel Fracture Technology Proves marginal Viking prospect Economic, Part II: Well Clean-up, Flowback and testing. Society of Petroleum Engineers. Doi:10.2118/36473-MS.

Harpel J.M., Barker L.B., Fontenot, J.M. 2012. Case History of the Fayetteville Shale Completions. Paper presented at the SPE Hydraulic Fracturing Technology Conference, The Woodlands, Texas, USA. Society of Petroleum Engineers SPE-152621-MS. DOI: 10.2118/152621-ms.

Hill A.C., and Thomas, G.W. 1985. A New Approach for Simulating Complex Fractured Reservoirs. Presented at the Middle East Oil Technical Conference and Exhibition, Bahrain, 11-14 March. SPE-13537-MS.

Hill H J, Klein G E, Shirley O J. 1979. Bound Water In Shaly Sands-Its Relation To Q And Other Formation Properties[J]. The log analyst, 20(03).

Holditch S.A. 1979. Factors Affecting Water Blocking and Gas Flow From Hydraulically Fractured Gas Wells. J pet Technol 31(12): 1515-1524. SPE-7561-PA. doi:10.2118/7561-PA.

Hui M., and Mallison, B. 2009. System and Method for Predicting Fluid Flow Characteristics Within Fractured Subsurface Reservoirs. US Patent Apple. 2009630709.

Hu J., He, S., Li, Y., et al. 2008. Study on the models for the forced flow-back of fracturing fluid and the backflow of proppant. [J]: Journal of Xi'an Shiyou University (Natural Science Edition). 2008(09), Vol23(5): 57-61.

Ilk D. and Currie S.M. 2010. A Comprehensive Work-flow for Early Analysis and interpretation of Flowback Data from Wells in Tight Gas/Shale Reservoir Systems. Presented at the SPE Annual Technical Conference and Exhibition, Florence, 19-22 September. SPE-135607-MS.

Jamiolahmady M., Aljmi, E. 2014. A Thorough Investigation of Clean-up Efficiency of Hydraulic Fractured Wells Using Statistical Approaches. Society of Petroleum Engineers. Doi:10.2118/170862-MS.

Jamiolahmady M., Sohrabi, M., & Danesh, A. 2007. Impact of Fracture Clean-up on Productivity of Gas-condensate Wells. Society of Petroleum Engineers. Doi:10.2118/107432-MS.

Jaripatke O., Grieser B. and Chong K.K. 2010. A Completions Road Map to Shale Play Development-Review of Successful Approach Towards Shale Play Stimulation in the Last Two Decades.SPe130369.

Jarvie D. M., Hill, R. J., Ruble, T. E., Pollastro, R. M., 2007. Unconventional shale-gas systems: the mississippian barnett shale of north-central texas as one model for thermogenic shale-gas assessment. AAPG Bulletin 91(4), 475-499.

Jiang T., Xu, Y., Zhang S. and Kang R. 2008. Optimization of Choke Size during Flowing Back After Hydraulic Fracturin. [J]: Petroleum Drilling Techniques, 2008(3),vol36(2): 54-59.

Jiang T., Wang, X., Guan, W. and Zeng, B. 2003. A New Analytical Model for Pressure Dectine under Condition of Forced Fracture Closure. [J]: Acta Petrolei Sinica. 2003(1), Vol24(1): 79-81.

Kamath J. and Laroche, C. 2003. Laboratory-Based Evaluation of Gas Well Deliverability Loss Caused by Water Blocking. SPE J. 8(1): 71-80. SPE-83659-PA. doi: 10.2118/83659-PA.

King G.E. 2010. Thirty Years of Gas Shale Fracturing: What Have We Learned? Paper presented at the SPE Annual Technical Conference and Exhibition, Florence, Italy. Society of Petroleum Engineers SPE-133456-MS. DOI: 10.2118/133456-ms.

Kaura, J.D., Macrae, A., & Mennie, D. 2001. Clean up and Well Operations in High-Rate Gas-Condensate Field Result in Improved Sand management System. Society of Petroleum Engineers. Doi:10.2118/68747-MS.

Korb J. P., Nicot, B., Louisjoseph, A., Bubici, S., Ferrante, G., 2014. Dynamics and wettability of oil and water in oil shales. Journal of Physical Chemistry C 118(40), 23212-23218.

Li F. (1980). Influence of Clay Minerals on Reservoir Properties in Sandstone Reservoirs [J]. Petroleum Exploration and Development, 45-51.

Li L., and Lee, S.H., and Eakin, B.E. 1966. The Viscosity of Natural Gases. Journal of Petroleum Technology. 18(08): 997-1000.

Li X., Hu, S., Cheng, K. 2007. Enlightenment of fractured shale gas exploration and development in North America. Petreleum Exploration and Development, 8(4). 392-400.

Liu H., Wang L. 2009. Discussion on Applicable Technology of Shale Gas Exploration and Development in China [J], Well Testing, 18(4): 68-71.

Lolon, E.P., McVay, D.A. 2003. Effect of Fracture conductivity of Effective Fracture Length. Paper SPE 84311 presented at the SPE Annual Technical Conference and Exhibition, Denver, 5-8 October. Doi:10.2118/84311-MS.

Ma C., Huang L. 2011. Gas Fracturing Technique for Shale and its Effect Evaluation [J]. Tuha Oil Gas, 16(3): 243-246.

Mahadevan, J., Le, D.H., and Hoang, H.N. 2009. Impact of Capillary Suction on Fracture Face Skin Evolution in Waterblocked Wells. Paper 119585 presented at the SPE Hydraulic Fracturing Technology Conference, The Woodlands, Texas, USA, 19-21 January. Doi:10.2118/119585-MS.

Makhanov, K., Dehghanpour, H., and Kuru, E. 2012. An Experimental Study of Spontaneous Imbibition in Horn River Shales. Paper SPE 162650 presented at SPE Canadian Unconventional Resources Conference, Calgary, Alberta, Canada, 30 October-1 November. http://dx.doi.org/10.2118/162650-MS.

May, E.A., Britt, L.K. and Nolte, K.G. 1997. The Effect of Yield Stress on Fracture Fluid Cleanup. Paper SPE 38619 presented at the SPE Annual Technical Conference and Exhibition, San Antonio, Texas, USA. 5-8 October. Doi: 10.2118/38619-MS.

Maxwell, S.C., Urbancic, T.I. 2002. Microseismic Imaging of Hydraulic Fracture Complexity in the Barnett Shale. Presented at the SPE Annual Technical Conference and Exhibition, San Antonio, 19 Septermber-2 October. SPE-77440-MS.

Mobil Annual Report 2007［R］. Mobil，2007.

Mohan, J., Sharma, M.M., & Pope, G.A. 2006. Optimization of Fracture Length in Gas/Condensate Reservoirs. Society of Petroleum Engineers. Doi:10.2118/100543-MS.

Monifar, A., Erdle J.C., and Patel, K. 2016. Comparison of Numerical vs Analytical Models for EUR Calculation and Optimization in Unconventional Reservoirs. Presented at SPE Low Perm Symposium, Denver, 5-6 May. SPE-180209-MS.

Moinfar, A., Varavei, A., and Sepehrnoori, K. 2014. Development of an Efficient Embedded Discrete Fracture Model for 3D Compositional Reservoir Simulation in Fractured Reservoirs. SPE Journal. 19(02): 289-303. SPE-154246-PA.

Moody, L.F. 1944. Friction Factors in Pipe Flow. Trans., ASME,

Nelson, P.H. 2009. Pore-throat Sizes in Sandstones, Tight Sandstones and Shales. AAPG Bulletin, v.93, No.3: 329-340.

Nie H., Zhang J. 2012, Calculation of Shale Gas Accumulation Conditions and Gas Content Taking the Lower Paleozoic in Sichuan Basin and Its Periphery as an Example [J], Geological Journal, 86(2): 350-361.

Noorishad, J. and Mehran, M. 1982. An Upstream Finite Element Method for Solution of Transient Transport Equation in Fractured Porous Media. Water Resources Research. 18(3):588-596.

Odusina, E., Sondergeld, C., and Rai, Chandra. 2011. NMR Study of Shale Wettability. Paper SPE 147371 presented at Canadian Unconventional Resources Conference, Alberta, Canada, 15-17 November. http://dx.doi.org/10.2118/147371-MS.

Olson, J.E. 1995. Fracturing From Highly Deviated and Horizontal Wells: Numerical Analysis of Non-planar Fracture Propagation. Presented at the Low-Permeability Reservoirs Symposium, Denver, 19-22 March. SPE-29573-MS.

Palisch, T.T., Vincent, M.C., and Handren, P.J. 2008. Slickwater Fracturing-Food for Thought. Paper SPE 115766 presented at the SPE Annual Technical Conference and Exhibition, Denver, 21-24 September. Doi: 10.2118/115766-MS.

Pan, Z., Connell, L. D., Camilleri, M., & Connelly, L. 2010. Effects of matrix moisture on gas diffusion and flow in coal. Fuel, 89(11), 3207-3217.

Penny, G.S., Dobkins, T.A., and Pursley, J.T. 2006. Field Study of Completion Fluids to Enhance Gas Production in the Barnett Shale. Paper presented at the SPE Gas Technology Symposium, Calgary, Alberta, Canada. Society of Petroleum Engineers SPE-100434-MS. DOI: 10.2118/100434-ms.

Ross J K D, Bustin R M. 2009. The importance of shale composition and pore structure upon gas storage potential of shale gas reservoirs[J].Marine and Petroleum Geology, 26; 916-927.

Roychaudhuri, B., Tsotsis, T., and Jessen, K. 2011. An Experimental and Numerical Investigation of Spontaneous Imbibition in Gas Shales. Paper SPE 147652 presented at SPE Annual Technical Conference and Exhibition, Denver, Colorado, USA, 30 October-2 November 2011. http://dx.doi.org/10.2118/147652-MS.

Ruppert L F, Sakurovs R, Blach T P. 2013. A USANS/SANS Study of the Accessibility of Pores in the Barnett Shale to Methane and Water[J]. Energy & Fuels, 27(2): 772-779.

Schein, G. 2005. The Application and Technology of Slickwater Fracturing. Paper SPE 108807 presented as a Distinguished Lecture during the 2004-2005 season.

Simon G J., Chengho L., Paul R. 2000. Interaction between growing channels in proppant packs: length and number of channels [C]. SPE International Symposium on Formation Damage Control. Lafayette, Louisiana: SPE.

Shanley, K. W., Cluff, R. M., and Robinson, J. W. 2004. Factors Controlling Prolific Gas Production from Low-Permeability Sandstone Reservoir: Implications for Resource Assessment, Prospect Development, and Risk Analysis. AAPG Bul. 88, 8(8):1083-1121. DOI: 10.1306/03250403051.

Sharma, M. and Agrawal, S. 2013. Impact of Liquid Loading in Hydraulic Fractures on Well Productivity. Paper presented at the 2013 SPE Hydraulic Fracturing Technology Conference, The Woodlands, TX, USA. Society of Petroleum Engineers SPE-163837-MS. DOI: 10.2118/163837-ms.

Shaoul, J.R., Zelm, L.F.V., and Pater, H.J.D. 2011. Damage Mechanisms in Unconventional Gas Well Stimulation - a New Look at an Old Problem. Paper presented at the SPE Middle East Unconventional Gas Conference and Exhibition, Muscat, Oman. Society of Petroleum Engineers SPE-142479-MS. DOI: 10.2118/142479-ms.

Song, W. 2013. Studies on Large Scale of Flowback of Fracturing fluid in Horizontal Wells. [J]: Testing of Oil and Gas Wells. 2013(8): 37-40.

Stroustrup, B. 1979. The C++ Programming Language-Reference Mannual. AT&T Bell Laboratories, Murray Hill, New Jersey 07974.

Sun W., Wang T., Liu Q. 1992. Physical and Chemical Properties of Clay [M]. Beijing Geological Publishing House, 36-40.

Tannich, J.D. 1975. Liquid Removal from Hydraulically Fractured Gas Wells. J Pet Technol 27 (11): 1309-1317. SPE-5113-PA. doi:10.2118/5113-PA.

Tuller, M., Or, D., Dudley, L. M., 1999. Adsorption and capillary condensation in porous media: liquid retention and interfacial configurations in angular pores. Water Resources Research 35(7), 1949-1964.

Vargaftik, N.B., Volkov, B.N. and Voljak, L.D. 1983. International Tables of the Surface Tension of Water. J.Phys.Chem.Ref.Data, Vol.12, No.3:817-820.

Wang, C., et al. 2014. Method to Optimize Choke Sizes During Back Flow. Science Technology and Engineering 14:010.

Wang, D., Butler, R., Liu, H. 2010. Flow Rate Behavior and Imbibition in Shale. Paper presented at the SPE Eastern Regional Meeting, Morgantown, West Virginia, USA. Society of Petroleum Engineers SPE-138521-MS. DOI: 10.2118/138521-ms.

Wang, H. and Zhang, S. 1998. [M]: Numerical Calculation Methodology of hydraulic Fracturing Design. Beijing: Petroleum Industry Press.

Wang, J.Y., Holditch, S., & Pope, G.A. 2006. Modeling Fracture-Fluid Cleanup in Tight-Gas Wells. Society of Petroleum Engineers. Doi:10.2118/119624-PA.

Wang X. 1992. Clay Minerals and Reservoir Protection in Sandstone Reservoirs [M]. Beijing Geological Publishing House, 409-492.

Warren, J.E. and root, P.J. 1963. The Behavior of Naturally Fractured Reservoirs. SPE Journal. 3(03): 245-255. SPE-426-PA.

Warpinski, N.R., Kramm, R.C. 2005. Comparison of Single- and Dual- Array Microseismic Mapping Techniques in the Barnett Shale. Paper SPE 95568 presented at the SPE Annual Technical Conference and Exhibition, Dallas, 9-12 October. Doi: 10.2118/95568/MS.

Williams-Kovacs, J., and Clarkson, C. 2016. A Modified Approach for Modeling Two-Phase Flowback from Multi-Fractured Horizontal Shale Gas Wells. Journal of Natural Gas Science and Engineering. 30:127-147.

Wu, K., and Olson, J.E. 2016. Numerical Investigation of Complex Hydraulic Fracture Development in Naturally Fractured Reservoirs. SPE Production & Operations. (Preprint). SPE-173326-PA.

Wu, K., and Olson, J.E. 2015. Simultaneous Multifracture Treatments: Fully Coupled Fluid Flow and Fracture Mechanics for Horzontal Wells. SPE Journal. 20(02): 337-346. SPE-167626-PA.

Xu, Y., Adefidipe, O.A., and Dehghanpour, H. 2015. Volumetric Analysis of Two-Phase Flowback Data for Fracture Characterization. Presented at the SPE Western Regional Metting, Garden Grove, 27-30 April. SPE-174023-MS.

Xu M, Dehghanpour H. 2014. Advances in understanding wettability of gas shales[J]. Energy & Fuels, 28(7): 4362-4375.

Yi, X. 2004. Model for Displacement of Herschel-Buckley Non-Newtonian Fluid by Newtonian Fluid in Porous Media and Its Application in Fracturing Fluid Cleanup. Paper SPE 86491 Presented at the SPE International Symposium and Exhibition on Formation Damage Control, Lafayette, Louisiana, USA. 18-20 February. Doi:10.2118/86491-MS.

Yuan W, Li X, Pan Z. 2014. Experimental investigation of interactions between water and a lower Silurian Chinese shale[J]. Energy & Fuels, 28(8): 4925-4933.

Yu, W. 2015. A Comprehensive Model for Simulation of Gas Transport in Shale Formation with Complex Hydraulic Fracture Geometry. Presented at the SPE Annual Technical Conference and Exhibition, Houston, 28-30 September. SPE-178747-STU.

Zhang J., Jin Z., Yuan M. 2004. Reservoiring mechanism of shale gas and its distribution. Natural Gas Industry. 24(7),15-18.

Zhang, K., Liu, Q., Wang, K. 2016. Optimization of choke Valves for Fracture Clean-up in Tight Gas Condensate Reservoirs. Presented at the SPE Annual Technical Conference and Exhibition, Denver, Colorado, USA, 5-6 May 2016. SPE-180275-MS.

Zhang, Y. 2013. Accounting for Remaining Injected Fracturing Fluid. MS Thesis, Texas A&M University, College Station, Texas (October, 2013).

Zhao X., Zhang Y. 1990. Clay minerals and Clay minerals Analysis[M].Beijing Maritime Press, 37-83; 131-149.

Zhou, M., Lu, D., Dunsmuir, J., and Thomann, H. 2000. Irreducible Water Distribution in Sandstone Rock: Two Phase Flow Simulations in CT-Based Pore Network. Physics and Chemistry of the Earth, Part A: Solid Earth and Geodesy, 25(2): 169-174.

Zhou, W., Banerjee, R. 2014. Semianalytical Production Simulation of Complex Hydraulic Fracture Networks. SPE Journal. 19(01): SPE-157367-PA.

Zou C. 2013. Unconventional Oil and Gas Geology [M]. Beijing Geological Publishing House.